



Repositorio Institucional de la Universidad Autónoma de Madrid

<https://repositorio.uam.es>

Esta es la **versión de autor** del artículo publicado en:

This is an **author produced version** of a paper published in:

Journal of Inorganic Biochemistry 138 (2014): 16-23

DOI: <http://dx.doi.org/10.1016/j.jinorgbio.2014.04.017>

Copyright: © 2014 Elsevier Inc. All rights reserved.

El acceso a la versión del editor puede requerir la suscripción del recurso

Access to the published version may require subscription

New bioactive 2,6-diacetylpyridine bis(*p*-chlorophenylthiosemicarbazone) ligand and its Pd(II) and Pt(II) complexes: synthesis, characterization, cytotoxic activity and DNA binding ability.

Ana I. Matesanz^{a*}, Carolina Hernández^{a,b} and Pilar Souza^a

^aDepartamento de Química Inorgánica (Módulo 07), Facultad de Ciencias, c/ Francisco Tomás y Valiente nº 7, Universidad Autónoma de Madrid, 28049-Madrid, Spain.

^bDepartamento de Química Inorgánica, Orgánica y Bioquímica, Facultad de Ciencias del Medio Ambiente, Avd. Carlos III s/n, Universidad de Castilla-La Mancha, 45071-Toledo, Spain.

Keywords: Antitumor activity, Asymmetric coordination, 2,6-Diacetylpyridine, Palladium and Platinum complexes, Thiosemicarbazone.

*Corresponding author. Tel.: +34 914973868; fax: +34 914974833. E-mail address: ana.matesanz@uam.es

Abstract

Preparation and characterization of 2,6-diacetylpyridine bis(⁴*N*-*p*-chlorophenylthiosemicarbazone) ligand, H₂L, and its palladium(II) and platinum(II) complexes [PdL] and [PtL], is described. The molecular structure of the two new complexes has been determined by single crystal X-ray diffraction. The ligand act as dianionic tetradentate donor coordinating to the metal center in a square planar geometry through the pyridine nitrogen atom and the azomethine nitrogen and thione sulfur atoms from one thiosemicarbazone arm, the fourth coordination position is occupied by the hydrazine nitrogen atom of the other arm. New free ligand and its metal complexes have been evaluated for antiproliferative activity *in vitro* against NCI-H460, T-47D, A2780 and A2780cisR human cancer cell lines. The cytotoxicity data suggest that these compounds may be endowed with important antitumor properties, especially H₂L and [PtL] since they are capable of not only circumvent cisplatin resistance in A2780cisR cells but also exhibit high antiproliferative activity in breast cancer T-47D cells. The interaction of H₂L with calf thymus DNA was also investigated and its binding constant (K_b) determined.

1. Introduction

Platinum metallo-drugs are among the most effective agents for the treatment of cancer however its clinical utility is restricted due to the frequent development of drug resistance, the limited spectrum of tumors against which these drugs are active and also the severe normal tissue toxicity [1-5]. These disadvantages have driven the development of improved platinum-based anticancer drugs whose structure and mode of action differ from that of cisplatin, especially those that interact with specific molecular targets as for example are the processes associated to DNA: transcription, replication and repair [6-9].

In this regard, of particular interest are compounds targeting ribonucleotide reductase (RR), enzyme that catalyzes the reduction of ribonucleotides to deoxyribonucleotides and provides the building blocks for the de novo DNA synthesis in all living cells. Cancer cells require increased RR activity to meet the demand for deoxyribonucleotides that are needed to support their rapid proliferation. Thus inhibition of RR activity leads to inhibition of DNA synthesis and repair, and also induces cell cycle arrest and apoptosis [10-12].

α -(N)-heterocyclic thiosemicarbazones, (N)-TSCs, have been reported to be among the most effective RR inhibitors yet identified and many efforts have been devoted to the study of the structure–activity relationship of thiosemicarbazone derivatives. The anticancer activity of (N)-TSCs is closely related to the nature of the heterocyclic ring of the parent aldehyde or ketone, metal chelation ability and terminal amino substitution [13-20]. In this sense pyridine ring itself is a part of many natural and synthetically prepared pharmaceuticals and moreover it plays a significant role in many biological processes like nicotinamide adenine dinucleotide phosphate NADP or the important vitamins niacin and pyridoxine (vitamins B3 and B6) [21, 22].

Keeping in view the above observations and as part of our systematic investigation on the coordination chemistry of thiosemicarbazone derivatives we recently reported palladium(II) and platinum(II) complexes derived of 2,6-diacetylpyridine bis(⁴*N*-*o*-tolylthiosemicarbazone) and 2,6-diacetylpyridine bis(⁴*N*-*p*-tolylthiosemicarbazone) ligands. The *in vitro* antitumor studies have shown that these complexes exhibit important antiproliferative activity in A2780 and A2780cisR human cancer cell lines and these results encouraged us to further investigate their cytotoxic properties as well as those of novel derivatives [23].

This work is aimed to determine if the presence of an aryl ring with an electron withdrawing substituent (such as *p*-chlorophenyl group) results beneficial for the antitumor activity of bis(⁴*N*-substituted thiosemicarbazones) ligands derived from 2,6-diacetylpyridine. Therefore here we describe the synthesis and chemical characterization of the new 2,6-diacetylpyridine bis(⁴*N*-*p*-chlorophenylthiosemicarbazone) ligand, H₂L, (Scheme 1) and its palladium(II) and platinum(II) complexes, [PdL] and [PtL].

Insert Scheme 1

The cytotoxic activity of the new compounds synthesized and cisplatin (assumed as the reference antitumor drug) against four human cancer cell lines: NCI-H460 (non-small cell lung cancer), T-47D (breast cancer), A2780 and A2780cisR (epithelial ovarian cancer) has been studied. The interaction of H₂L with calf thymus DNA (CT-DNA) was also investigated and its binding constant (K_b) determined.

2. Experimental

2.1. Measurements

Elemental analyses were performed on a LECO CHNS-932 microanalyzer. Fast atom bombardment (FAB) mass spectra (MS) were performed on a VG AutoSpec spectrometer. ^1H NMR spectra were recorded on Bruker AMX-300 spectrometer. All cited physical measurements were obtained out by the Servicio Interdepartamental de Investigación (SIdI) of the Universidad Autónoma de Madrid.

Melting points were determined with a Stuart Scientific SMP3 apparatus. Infrared spectra were recorded on a Bomen–Michelson spectrophotometer. ^{13}C NMR spectra were recorded on a 400 Advance Bruker Fourier Transform spectrometer. Electronic spectra were recorded on a Thermo Scientific Evolution 260 Bio UV-visible (UV-VIS) spectrophotometer.

2.2. Materials

Solvents were purified and dried according to standard procedures. Hydrazine hydrate, 2,6-diacetylpyridine, *p*-chlorophenyl isothiocyanate, $\text{PdCl}_2(\text{PPh}_3)_2$ and $\text{PtCl}_2(\text{PPh}_3)_2$ were commercially available.

2.3. Synthesis of compounds

2,6-Diacetylpyridine bis(4N -*p*-chlorophenylthiosemicarbazone), H_2L . An ethanolic solution of hydrazine hydrate (0.250 g, 5 mmol) was added dropwise with constant stirring to an ethanolic solution of *p*-chlorophenyl isothiocyanate (0.848 g, 5 mmol). The reaction mixture was stirred for one more hour and then the white product *p*-chlorophenylthiosemicarbazide formed was filtered, washed with cold ethanol and diethyl ether, dried *in vacuo* and recrystallized from ethanol. An ethanolic solution of the *p*-chlorophenylthiosemicarbazide (0.402 g, 2 mmol) was then stirred with 2,6-diacetylpyridine (0.163 g, 1 mmol) for 5 h. The resulting solution was reduced to half

volume and the pale yellow solid formed was filtered, washed with ethanol, diethyl ether and finally dried *in vacuo*.

Yield (80%), mp 220 °C (decomposes). Elemental analysis found, C, 52.20; H, 4.25; N, 18.00; S, 12.20; C₂₃H₂₁N₇S₂Cl₂ requires C, 52.07; H, 3.99, N, 18.48; S, 12.09 %. MS (FAB⁺ with *m*NBA: nitrobenzyl alcohol matrix) *m/z* 530.0 for [H₂L+H]⁺. IR (KBr pellet): ν/cm⁻¹ 3335, 3306, 3210 (w, NH); 1588 (s, CN); 827, 809 (w, CS-thioamide IV); 585 (pyridine ring). ¹H NMR (d⁶-DMSO, ppm), δ=10.80 [s, ²NH, 2H]; 10.20 [s, ⁴NH, 2H]; 8.55 [d, *J*=7.9 Hz, CH-pyridine, 2H]; 7.85 [t, *J*=7.9 Hz, CH-pyridine, 1H]; 7.60 (d, *J*=8.7 Hz, aromatic-thiosemicarbazide, 4H); 7.45 (d, *J*=8.7 Hz, aromatic-thiosemicarbazide, 4H); 2.50 (s, CH₃-diacetylpyridine, 6H). ¹³C NMR (d⁶-DMSO, ppm), δ=178.3 (C=S); 153.78 (C2,C6-pyridine); 149.85 (C=¹N); 138.54 (C4-pyridine); 137.17 (C3,C5-pyridine); 130.08 (aromatic-thiosemicarbazide); 128.49 (aromatic-thiosemicarbazide); 128.34 (aromatic-thiosemicarbazide); 127.37 (aromatic-thiosemicarbazide); 121.96 (aromatic-thiosemicarbazide); 12.98 (CH₃-diacetylpyridine). UV/VIS (DMSO): λ/nm 250, 337.

2,6-Diacetylpyridine bis(⁴N-*p*-chlorophenylthiosemicarbazonato)palladium(II), [PdL]. The reaction of H₂L ligand with PdCl₂(PPh₃)₂, in toluene, in presence of Et₃N, in 1:1 molar ratios over 20 h at room temperature led to the formation of an orange solution which was filtered and left to stand at ambient temperature for two days. The brown solid formed was filtered, washed several times with hot water, diethyl ether and finally dried *in vacuo*.

Yield (55%), mp >250 °C. Elemental analysis found, C, 43.35; H, 3.35, N, 15.10; S, 10.05; C₂₃H₁₉N₇S₂Cl₂Pd requires C, 43.51; H, 3.02, N, 15.44; S, 10.10 %. MS (FAB⁺ with *m*NBA matrix) *m/z* 636 for [PdL+H]⁺. IR (KBr pellet): ν/cm⁻¹ 3243 (s, NH); 1595 (s, CN); 830, 804 (vw) (CS-thioamide IV); 603 (pyridine ring). ¹H NMR (300 MHz, d⁶-

DMSO, ppm), δ =10.75, 10.18 [s, ^4NH , 2H]; 8.43-8.10 [m, CH-pyridine, 3H]; 7.71-7.34 (m, aromatic-thiosemicarbazide, 8H); 2.72, 2.62 (s, CH_3 -diacetylpyridine, 6H). UV/VIS (DMSO): λ/nm 267, 340, 410, 470.

Recrystallization from DMSO led to the isolation of orange crystals of $[\text{PdL}]\cdot\text{DMSO}$ that were suitable for X-ray-diffraction.

2,6-Diacetylpyridine bis(^4N -*p*-chlorophenylthiosemicarbazonato)platinum(II), [PtL]. It was prepared by the same procedure as described for [PdL] by reaction of H_2L with $\text{PtCl}_2(\text{PPh}_3)_2$ and afforded a brown solid.

Yield (35%), mp 192 °C (decomposes). Elemental analysis found, C, 37.90; H, 2.55, N, 13.60; S, 8.60; $\text{C}_{23}\text{H}_{19}\text{N}_7\text{S}_2\text{Cl}_2\text{Pt}$ requires C, 38.18; H, 2.65, N, 13.55; S, 8.86 %. MS (FAB^+ with *m*NBA matrix) m/z 724 for $[\text{PtL}+\text{H}]^+$. IR (KBr pellet): ν/cm^{-1} 3288, 3208 (s, NH); 1590 (s, CN); 826, 809 (vw) (CS-thioamide IV); 591 (pyridine ring). ^1H NMR (300 MHz, d^6 -DMSO, ppm), δ =11.00, 10.30 [s, ^4NH , 2H]; δ =8.56-8.10 [m, CH-pyridine, 3H]; δ =7.76-7.70 (m, aromatic-thiosemicarbazide, 8H); δ =2.78, 2.71 (s, CH_3 -diacetylpyridine, 6H). UV/VIS (DMSO): λ/nm 249, 267, 366.

Recrystallization from DMSO led to the isolation of orange crystals of $[\text{PtL}]\cdot\text{DMSO}$ that were suitable for X-ray-diffraction.

2.4. Crystallography

Data were collected on a Bruker X8 APEX II CCD. Crystallographic data and selected interatomic distances and angles are listed in Table 1. For all compounds, the software package SHELXTL was used for space group determination, structure solution, and refinement [24]. The structures were solved by direct methods, completed with difference Fourier syntheses, and refined with anisotropic displacement parameters.

CCDC 981268 and 981269 contain the supplementary crystallographic data for compounds [PdL] and [PtL] respectively. These data can be obtained free of charge at www.ccdc.cam.ac.uk/conts/retrieving.html [or from the Cambridge Crystallographic Data Centre, 12, Union Road, Cambridge CB2 1EZ, UK; fax: +44-1223/336-033; e-mail: deposit@ccdc.cam.ac.uk].

2.5. *In vitro* antiproliferative activity

The human cancer cells: A2780 and A2780cisR (epithelial ovarian cancer), T-47D (breast cancer) and NCI-H460 (non-small cell lung cancer); were grown in RPMI-1640 medium supplemented with 10% foetal bovine serum (FBS) and 2 mM L-glutamine in an atmosphere of 5% CO₂ at 37 °C.

Cell proliferation was evaluated by the sulforhodamine B assay. Cells were plated in 96-well sterile plates at a density of 1.5×10^4 (for NCI-H460), 4×10^3 (for A2780 and A2780cisR) or 5×10^3 (for T-47D) cells per well with 100 μ L of medium and were then incubated for 24 h (A2780, A2780cisR and NCI-H460) or 48 h (T-47D). After attachment to the culture surface the cells were incubated with various concentrations of the compounds tested freshly dissolved in DMSO (1 mg/mL) and diluted in the culture medium (DMSO final concentration 1%) for 48 h (for NCI-H460) or 96 h (for A2780, A2780cisR and T-47D). The cells were fixed by adding 50 μ L of 30% trichloroacetic acid (TCA) per well.

The plates were incubated at 4 °C for 1 h and then washed five times with distilled water. The cellular material fixed with TCA was stained with 0.4% sulforhodamine B dissolved in 1% acetic acid for 10 min. Unbound dye was removed by rinsing with 0.1% acetic acid. The protein-bound dye was extracted with 10 mM unbuffered Tris base for determination of optical density (at 515 nm) in a Tecan Ultra Evolution spectrophotometer.

The effects of compounds were expressed as corrected percentage inhibition values according to the following equation:

$$\% \text{ inhibition} = [1 - (T/C)] \times 100$$

where T is the mean absorbance of the treated cells and C the mean absorbance in the controls.

The inhibitory potential of compounds was measured by calculating concentration–percentage inhibition curves, these curves were adjusted to the following equation:

$$E = E_{\max} / [1 + (IC_{50}/C)^n]$$

where E is the percentage inhibition observed, E_{\max} is the maximal effects, IC_{50} is the concentration that inhibits 50% of maximal growth, C is the concentration of compounds tested and n is the slope of the semi-logarithmic dose–response sigmoid curves. This non-linear fitting was performed using GraphPad Prism software [25].

For comparison purposes, the antiproliferative activity of cisplatin was evaluated under the same experimental conditions. All compounds were tested in two independent studies with triplicate points. These experiments were carried out at the Unidad de Evaluación de Actividades Farmacológicas de Compuestos Químicos (USEF), Universidad de Santiago de Compostela.

2.6. DNA-Binding Experiments

Calf thymus DNA (CT-DNA) stock solution was prepared by dissolving the lyophilized sodium salt in Tris-buffer (NaCl 50 mM, Tris-HCl 5 mM, pH was adjusted to 7.2 with NaOH 0.5 M) by stirring for 5 hours. The CT-DNA solution was standardized spectrophotometrically [26] by using its known molar absorption coefficient at 260 nm ($6600 \text{ M}^{-1} \cdot \text{cm}^{-1}$). The ratio of UV absorbance at 260 and 280 nm,

A_{260}/A_{280} , of *ca.* 1.9, indicating that the DNA was sufficiently free of protein. Stock solution was kept frozen until the day of the experiment.

Concentrated stock solutions (5×10^{-3} M and 5×10^{-5} M) of H₂L were prepared dissolving the compound in DMSO. From these stock solutions, for all experiments the desired concentration of compound was achieved by dilution with Tris-buffer (NaCl 50 mM, Tris-HCl 5 mM, pH was adjusted to 7.2 with NaOH 0.5 M) to give homogeneous solutions with DMSO content of less than 2.5 %.

To investigate the binding mode, spectrophotometric titrations were performed at a fixed DNA concentration equal to 1.7×10^{-4} M with increasing concentration of H₂L (0-125 μ M) and monitoring the absorbance change at the wavelength maximum 260 nm after incubation (10 min. at 37°C).

To calculate the binding parameters, the spectrophotometric titrations were performed with increasing concentration of DNA (0-40 μ M) at a fixed compound concentration equal to 50 μ M and monitoring the absorbance change in one characteristic charge transference band of the compound after incubation (10 min. at 37°C).

3. Results and discussion

3.1. Synthesis and spectroscopic characterization

A new 2,6-diacetylpyridine bis(⁴N-monosubstituted thiosemicarbazone) ligand has been synthesized with high purities and acceptable yields. The yellow compound obtained is stable to air and moisture and was characterized by elemental analysis, FAB⁺ spectrometry and IR and NMR (¹H and ¹³C) spectroscopy.

Reaction of 2,6-diacetylpyridine bis(⁴N-*p*-chlorophenylthiosemicarbazone) ligand with equimolar amount of $MCl_2(PPh_3)_2$, where M = Pd(II) or Pt(II), led to the

isolation of neutral mononuclear complexes [PdL] and [PtL] in which the bis(thiosemicarbazone) behaves as dianionic ligand with deprotonation of hydrazine (^2NH) protons and [NNNS] donor set.

Both complexes were characterized by routine analytical and spectroscopic techniques. Analytical data are consistent with the formulation given, thus the FAB⁺ mass spectra exhibited a very weak ion at $m/z = 636$ for [PdL] and $m/z = 724$ for [PtL] which corresponded to the predicted molecular weight of the $[\text{M}+\text{H}]^+$ ions and moreover the isotopic patterns of this signal fit well with the theoretical isotopic distributions.

The significant IR vibrational bands and the ^1H chemical shift values of the free ligand and its complexes are listed in the Experimental section and Scheme 1 shows the numbered structure of the free ligand. As the X-ray study has shown, during metal complexation, the ligand behaves as a tetradentate dianionic forming two five-membered and one six-membered chelate rings around the metal center. The high delocalization and the asymmetric coordination hinder the IR analysis. The stretching vibration $\nu(\text{C}=\text{N})$ and the in-plane pyridine deformation bands are slightly shifted to higher wavenumbers which are consistent with the implication of imine and pyridine nitrogen atoms in the coordination however this induces only minor changes in $\nu(\text{C}=\text{S})$ thioamide IV band which decreases slightly in intensity.

In the ^1H NMR spectrum of the double-armed H_2L ligand, two independent singlets at $\delta = 10.80$ and 10.20 ppm are observed for $>\text{C}=\text{N}-^2\text{NH}-$ and $-\text{C}(\text{S})-^4\text{NH}-$ protons respectively. A doublet at $\delta = 8.55$ ppm and a triplet at $\delta = 7.85$ ppm are assigned to pyridyl ring protons. Aromatic *p*-chlorophenyl protons appear as a multiplet at $\delta = 7.60\text{--}7.45$ ppm and a sharp singlet at $\delta = 2.50$ is assigned to the methyl protons. In [PdL] and [PtL] complexes, the anionic coordination of the ligand is evidenced by

the disappearance of the signal corresponding to the $>\text{C}=\text{N}-^2\text{NH}-$ protons. On the other hand, the $-\text{C}(\text{S})-^4\text{NH}-$ protons appear two independent signals (10.75 and 10.18 ppm for [PdL] and 11.00 and 10.30 ppm for [PtL]) due to the asymmetric coordination. The pyridyl ring protons appear as a multiplet at $\delta = 8.43\text{-}8.10$ ppm for [PdL] and $\delta = 8.56\text{-}8.10$ ppm for [PtL] and the rest of the proton signals appear at nearly identical positions if they are compared with the corresponding ligand signals.

^{13}C NMR spectrum of the free ligand shows carbon signals supporting the ^1H NMR assignments however due to the low solubility of the complexes it was not possible to get ^{13}C NMR spectra of reasonably quality.

The electronic absorption spectra of both $[\text{H}_2\text{L}]$ ligand and [PdL] and [PtL] complexes exhibit two intense band in the region 250-400 nm, which can ascribed to ligand-centered $n\rightarrow\pi^*$ and $\pi\rightarrow\pi^*$ transitions. In addition the spectra of metal complexes exhibit other less energetic bands assigned to a ligand to metal (LMCT) and metal to ligand charge transfer (MLCT) transitions [27].

3.2. Description of the crystal structures

[PdL]·DMSO and **[PtL]·DMSO** were isolated as neutral compounds. The most significant crystallographic data for these complexes are shown in Table 1, whereas selected bond lengths and bond angles are presented in Table 2.

Insert Table 1

The structures together with the atom labeling schemes are shown in Figures 1 and 2. Both compounds are isostructural hence displaying nearly identical cell parameters, crystallize in the triclinic $P\bar{1}$ space group with $Z=2$ and the asymmetric units

contain one molecule of the neutral complex and one dimethyl sulfoxide solvent molecule.

Insert Figure 1

Insert Figure 2

The metal ion presents a square planar geometry where the bis(thiosemicarbazone) ligand is coordinated to the metal ion through the pyridine nitrogen atom and the azomethine nitrogen and thione sulfur atoms from one thiosemicarbazone arm and being the fourth coordination position occupied by the hydrazine nitrogen atom of the other thiosemicarbazone arm generating two typical five membered (PdSCNN and PdNCCN or PtSCNN and PtNCCN) and one six membered (PdNNCCN or PtNNCCN) chelate rings. Coordination by hydrazine nitrogen atom instead of the azomethine nitrogen atom, although uncommon, has been found in the bibliography for some d⁸ bis(thiosemicarbazone) complexes [23, 28-31].

The M–N and M–S bond distances are similar to those found in other palladium(II) and platinum(II) complexes. It is important to note that the two thiosemicarbazone moieties, which are symmetrically deprotonated, coordinate in a different fashion. Upon coordination the bidentate-N,S arm undergoes significant evolution from the thione to the thiol form which is reflected in C–S distance of 1.779(4) for [PdL]·DMSO and 1.804(10) for [PtL]·DMSO while the monodentate-thiosemicarbazone [N(3), hydrazine nitrogen atom] arm maintains its thione form as reflects in their C–S bond length of 1.673(5) for [PdL]·DMSO and 1.672(3) Å for [PtL]·DMSO, typical of double C=S bond.

Insert Table 2

Comparison of C–N and N–N bond distances with typical lengths of single and double bonds [C–N 1.47, C=N 1.28, N–N 1.45, N=N 1.25 Å] suggests extensive charge delocalization over the thiosemicarbazone moieties [32, 33] and also agree with the thiolate tautomeric form of the bidentate thiosemicarbazionate arm and the thione tautomeric form of the monodentate one (Scheme 2).

Insert Scheme 2

Inspection of the angles formed between the metal ion ($M = Pd^{2+}$, Pt^{2+}) and the coordinated atoms shows that the metal is contained within a slightly distorted square-planar environment being the bond angles between adjacent coordinating atoms in the 80.5–104.2° range.

The crystal structures are stabilized by intermolecular hydrogen interactions involving the N(7) atom of the bidentate thiosemicarbazionate arms and the oxygen atom of DMSO solvent molecule being the N(7)–H(7)···O(1) contact distance 2.83 Å for both complexes and $\angle(NHO)$ angle 170.4° for [PdL] and 169.2° for [PtL]. Further stabilization of the crystal packing is provided by intermolecular π – π stacking interactions involving the whole planar bis(thiosemicarbazone)-metal skeleton (Figure 3), with an interplane separation about ≈ 3.5 Å.

Insert Figure 3

3.3. In vitro antiproliferative activity

To assess the antitumor potential of the synthesized compounds, its antiproliferative activity (in powder solid form) was tested *in vitro* against a panel of human cancer cells lines containing examples of lung (NCI-H460), breast (T-47D) and

ovarian (A2780 and A2780cisR) cancers. For comparison purposes, the cytotoxicity of cisplatin was always evaluated under the same experimental conditions.

Table 3 shows that both the *p*-chlorophenyl substituted free ligand H₂L and its platinum(II) complex [PtL] present important antiproliferative activity in the low-micromolar range, against ovarian (A2780, cisplatin sensitive, and A2780cisR, cisplatin resistant) and breast (T-47D) cancer cells. It is remarkable to note that both compounds exhibit better cytotoxic effects against T-47D cells than cisplatin by comparing their IC₅₀ values.

The A2780cisR cell line encompasses all of the known major mechanisms of resistance to cisplatin: reduced drug transport, enhanced DNA repair/tolerance, and elevated GSH levels. The ability of H₂L and [PtL] compounds to circumvent cisplatin-acquired resistance was confirmed from the resistance factor values, RF (defined as IC₅₀ in A2780cisR/IC₅₀ in A2780) since both have a much better RF value than cisplatin. An RF value of < 2 was considered to denote non-cross-resistance and therefore these compounds are able to circumvent cisplatin resistance [34,35].

From a chemical point of view, analysis of these data together with those of our previous study [23] in which the related ligand 2,6-diacetylpyridine bis(⁴*N*-*p*-tolylthiosemicarbazone), H₂L², resulted inactive in both A2780 and A2780cisR cell lines and its [PtL²] complex showed a slightly lower antiproliferative activity than [PtL] complex (see table 3) suggests that the presence of one electron withdrawing group attached to the ⁴N atom of the thiosemicarbazone moiety results beneficial for the antiproliferative activity of the bis(thiosemicarbazone) ligands of the 2,6-diacetylpyridine series.

Insert Table 3

3.4. DNA Interaction Studies

In order to initially address if any direct interaction with DNA is part of the mechanism of action of the compounds, UV-visible absorption spectra in absence and presence of CT-DNA were carried out for H₂L ligand, which have a significant effect against the tested cell lines.

Absorption spectral studies

The binding affinity between DNA and H₂L ligand can be detected by UV-Vis absorption spectroscopy by measuring the changes in the absorption properties of: a) DNA (for a variable H₂L concentration) or b) H₂L ligand molecule (for a variable DNA concentration).

The UV-Vis absorption spectrum of the typical β -form DNA exhibits a characteristic $\pi \rightarrow \pi^*$ band at 260 nm as consequence of the chromophoric groups in purine and pyrimidine moieties. Compounds binding with DNA through intercalation are consistent with hypochromism (decrease in DNA band absorption), resulted of a stacking interaction between the aromatic ligand chromophore and the base pair of DNA. In case of compounds binding with DNA through external contact (including groove binding and electrostatic attraction) usually hyperchromism (increase in DNA band absorption) is observed which is attributable of a contraction and overall damage of the secondary structure of DNA [36].

Thus, the absorption spectrum of CT-DNA in presence of H₂L was recorded, by keeping constant CT-DNA concentration (1.7×10^{-4} M) in diverse [CT-DNA]/[H₂L] mixing ratios ($R = 0.5-1.5$) and monitoring the change in the absorption intensity of the typical CT-DNA spectral band at 260 nm. As Figure 4 shows, when the concentration of H₂L is gradually increased a significant increase in absorption of the DNA band

occurs being the percentage of hyperchromism observed [% hyperchromism = $(A_{\text{DNA bound}} - A_{\text{DNA free}}) / A_{\text{DNA bound}}$] about 40 %.

Insert Figure 4

These characteristics suggest non-covalent surface (major or minor groove) binding along outside of DNA helix. The above observations are comparable to those reported earlier for various neutral bis(thiosemicarbazone) palladium and platinum complexes [37, 38].

The H₂L ligand exhibit, in DMSO:Tris buffer (2.5:100) mixture, one broad intense band of intraligand π - π^* transition at 250 nm and other less intense of intraligand n- π^* transition at 337 nm and any interaction with DNA could perturb it.

Thus, in order to determine the intrinsic binding constant (K_b), absorption titration experiments were performed by maintaining a constant H₂L concentration (50 μ M) while gradually increasing the concentration of DNA (0 - 40 μ M) and monitoring the change in the absorption intensity of the intraligand charge transfer band. While measuring the absorption spectra, an equal amount of DNA was added to both the test solution and the reference solution to eliminate the absorbance of DNA itself. The data were then fitted to the following equation, that is only valid for low compound:DNA ratios (i.e., far from the DNA saturation) and assumes no binding cooperativity [39]:

$$[\text{DNA}] / (\epsilon_a - \epsilon_f) = [\text{DNA}] / (\epsilon_b - \epsilon_f) + 1 / \{K_b (\epsilon_b - \epsilon_f)\}$$

where [DNA] is the concentration of the nucleic acid in base pairs, ϵ_a is the apparent absorption coefficient obtained by calculating $A_{\text{obs}}/[\text{compound}]$, and ϵ_f and ϵ_b are the absorption coefficients of the free and the fully bound compound, respectively.

A plot (Figure 5) of $[\text{DNA}]/(\epsilon_b - \epsilon_f)$ versus $[\text{DNA}]$, gives a slope of $1/(\epsilon_b - \epsilon_f)$ and a Y-intercept equal to $1/\{K_b(\epsilon_b - \epsilon_f)\}$. The intrinsic binding constant K_b is calculated as the ratio of the slope to the Y-intercept.

Insert Figure 5

On titration of CT-DNA a slight increase in the absorptivity of this band is observed which is indicative of interaction between the electronic states of the ligand chromophore with that of DNA bases. The magnitude of intrinsic binding constant was calculated to be $7.03 \times 10^4 \text{ M}^{-1}$ (correlation coefficient $R^2 = 0.99$) which is modest, however it should be kept in mind that the biological activity of α -(N)-heterocyclic thiosemicarbazones is not only due to their non-covalent DNA binding but they are also potent inhibitors of DNA synthesis and repair through RR inactivation. This fact could explain the good cytotoxic activity that both free ligand and platinum complex have demonstrated. Further studies and more practical experiments are required to elucidate the biochemical mechanisms involved in their activity.

4. Conclusions

A new family of Pt(II) and Pd(II) bis(thiosemicarbazone) compounds of the 2,6-diacetylpyridine series containing an aryl ring with an electron withdrawing substituent (*p*-chlorophenyl group) has been successfully prepared and characterized.

This study has identified both the free ligand H_2L and the Pt(II) complex $[\text{PtL}]$ as having high antiproliferative activity since they are capable of not only circumvent cisplatin resistance in A2780cisR cells but they also exhibit high antiproliferative activity against breast (T-47D) cancer cells.

Acknowledgments

We are grateful to Ministerio de Economía y Competitividad, Instituto de Salud Carlos III of Spain (PI1100659) for financial support.

References

- [1] N.J. Wheate, S. Walker, G.E. Craig, R. Oun, Dalton Trans. 39 (2010) 8113-8127.
- [2] E. Wong, C.M. Giandomenico, Chem. Rev. 99 (1999) 2451-2466.
- [3] Z. Guo, P.J Sadler, Angew. Chem. Int. Ed. 38 (1999) 1512-1531.
- [4] M.S. Razzaque, Nephrol. Dial. Transplant. (2007) 1-5.
- [5] M. Okuda, K. Masaki, S. Fukatsu, Y. Hashimoto, K. Inui, Biochem. Pharmacol. 59 (2000) 195–201.
- [6] K. van der Schilden, F. García, H. Kooijman, A.L. Spek, J.G. Haasnoot, J. Reedijk, Angew. Chem. Int. Ed. 43 (2004) 5668-5670.
- [7] L.H. Hurley, Nature Reviews Cancer, 2 (2002) 188-200.
- [8] T.W. Hambley, Coord. Chem. Rev. 166 (1997) 181-223.
- [9] J. Kasparkova, V. Marini, Y. Najajreh, D. Gibson, V. Brabec, Biochemistry 42 (2003) 6321-6332.
- [10] J. Shao, X. Liu, L. Zhu, Y. Yen, Expert. Opin. Ther. Targets 17 (2013) 1423-1437.
- [11] D.S. Kalinowski, D.R. Richardson, Pharmacol. Rev. 57 (2005) 547–583.
- [12] C. Kunos, T. Radivoyevitch, F.W. Abdul-Karim, J. Fanning, O. Abulafia, A.J. Bonebrake, L. Usha, J. Transl. Med. (2012) 10:79.
- [13] L. Zhu, B. Zhou, X. Chen, H. Jiang, J. Shao, Y. Yen, Biochem Pharmacol. 78 (2009) 1178-1185.
- [14] M. Liu, T. Lin, A.C. Sartorelli, Prog. Med. Chem. 32 (1995) 1-35.
- [15] D.X. West, A.E. Liberta, S.B. Padhye, R.C. Chikate, P.B. Sonawane, A.S. Kumbhar, R.G. Yerande, Coord. Chem. Rev. 123 (1993) 49.
- [16] A.I. Matesanz, P. Souza, Mini-rev. Med. Chem. 9 (2009) 1389-89.
- [17] C.R. Kowol, R. Berger, R. Eichinger, A. Roller, M.A. Jakupec, P. Schmidt, V.B. Arion, B.K. Keppler, J. Med. Chem. 50 (2007) 1254-1265.

- [18] R. A. Finch, M. C. Liu, A. H. Cory, J. G. Cory and A. C. Sartorelli, *Adv. Enzyme Regul.* 39 (1999) 3–12.
- [19] P. Heffeter, C. Pirker, C.R. Kowol, G. Herrman, R. Dornetshuber, W. Miklos, U. Jungwirth, G. Koellensperger, B.K. Keppler, W. Berger, *Biochem. Pharmacol.* 83 (2012) 1623-1633.
- [20] E. Ramachandran, D.S. Raja, J.L. Mike, T.R. Wagner, M. Zellerb, K. Natarajan, *RSC Adv.* 2 (2012) 8515–8525.
- [21] E. Lukevits, *Chem. Heterocyc. Comp.* 31 (1995) 639–650.
- [22] L.E. Kapinos, H. Sigel, *Inorg. Chim. Acta* 337 (2002) 131-142.
- [23] A.I. Matesanz, I. Leitaó, P. Souza, J. Inorg. Biochem. 125 (2013) 26–31.
- [24] SHELXTL-NT version 6.12, Structure Determination Package, Bruker-Nonius AXS, Madison, Wisconsin, USA, 2001.
- [25] GraphPad Prism, version 2.01, GraphPad Software, Inc., San Diego, CA, 1996.
- [26] M.A. Ali, A.H. Mirza, A.L. Tan, L.K. Wei, P.V. Bernhardt, *Polyhedron* 23 (2004) 2037–2043.
- [27] A.A. Ali, H. Nimir, C. Aktas, V. Huch, U. Rauch, K. Schäfer, M. Veith, *Organometallics*, 31 (2012) 2256–2262.
- [28] A.I. Matesanz, P. Souza, *Inorg. Chem. Commun.* 27 (2013) 5–8.
- [29] C.A. Brown, W. Kaminsky, K.A. Claborn, K.I. Goldberg, D.X. West, J. Braz. Chem.Soc. 13 (2002) 10–18.
- [30] J.I. Gradinaru, S.T. Malinowski, M.A. Popovici, M. Gdaniec, *Crystallogr. Rep.* 50 (2005) 217–223.
- [31] T.R. Todorović, A. Bacchi, G. Pelizzi, N.O. Juranić, D.M. Sladić, I.D. Brčeski, K.K. Anelković, *Inorg. Chem. Commun.* 9 (2006) 862–865.
- [32] R. Pedrido, A.M. González-Noya, M.J. Romero, M. Martínez-Calvo, M. Vázquez

- López, E. Gómez-Fórneas, G. Zaragoza, M.R. Bermejo, Dalton Trans. (2008) 6776–6787.
- [33] J.S. Casas, M.S. García-Tasende, J. Sordo, Coord. Chem. Rev. 209 (2000) 197–261.
- [34] L.R. Kelland, C.F.J. Barnard, K.J. Mellish, M. Jones, P.M. Goddard, M. Valenti, A. Bryant, B.A. Murrer, K.R. Harrap, Cancer Res. 54 (1994) 5618–5622.
- [35] J. Ruiz, C. Vicente, C. Haro, D. Bautista, Inorg. Chem. 52 (2013) 974–982.
- [36] F. Arjmand and M. Aziz, Eur. J. Med. Chem., 2009, 44, 834–844.
- [37] A.I. Matesanz, C. Hernández, A. Rodríguez, P. Souza, Dalton Trans. 40 (2011) 5738–5745.
- [38] A.I. Matesanz, J. Perles, P. Souza, Dalton Trans. 41 (2012) 12538–12547.
- [39] B. Pedras, R.M.F. Batista, L. Tormo, S.P.G. Costa, M.M.M. Raposo, G. Orellana, J.L. Capelo, C. Lodeiro, Inorg. Chim. Acta, 381 (2012) 95–103.

CAPTIONS

Scheme 1. Structure of 2,6-diacetylpyridine bis(⁴*N*-*p*-chlorophenylthiosemicarbazone), H₂L ligand.

Scheme 2. Delocalization System in the Thiosemicarbazone moiety

Figure. 1. Molecular structure of [PdL]. The displacement ellipsoids are drawn at the 50% probability.

Figure. 2. Molecular structure of [PtL]. The displacement ellipsoids are drawn at the 50% probability.

Figure. 3. Crystal packing view of [PdL]·DMSO along a axis, dashed lines denote $\pi\cdots\pi$ interactions.

Figure. 4. UV absorption spectrum of CT-DNA in the absence (black curve) and presence of increasing amounts of compound H₂L. The data were collected for [CT-DNA] = 1.7×10^{-4} M and [H₂L] = 0, 2.5×10^{-6} , 6.0×10^{-5} , 8.0×10^{-5} , 1.25×10^{-4} M (the arrow shows the changes upon increasing amounts of complex).

Figure. 5. UV absorption spectrum of H₂L in the absence (black curve) and presence of increasing amounts of compound CT-DNA. The data were collected for [H₂L] = 5×10^{-5} M and [CT-DNA] = 0, 20×10^{-6} , 60×10^{-6} , 70×10^{-6} , 75×10^{-6} M. The insert shows a fitting of the absorbance data used to obtain the binding constants.

**New bioactive 2,6-diacetylpyridine bis(*para*-chlorophenylthiosemicarbazone)
ligand and its Pd(II) and Pt(II) complexes: synthesis, characterization, cytotoxic
activity and DNA binding ability.**

Ana I. Matesanz^{a*}, Carolina Hernández^{a,b} and Pilar Souza^a

^aDepartamento de Química Inorgánica (Módulo 07), Facultad de Ciencias, c/ Francisco Tomás y Valiente nº 7, Universidad Autónoma de Madrid, 28049-Madrid, Spain.

^bDepartamento de Química Inorgánica, Orgánica y Bioquímica, Facultad de Ciencias del Medio Ambiente, Avd. Carlos III s/n, Universidad de Castilla-La Mancha, 45071-Toledo, Spain.

Keywords: Antitumor activity, Asymmetric N₃S coordination, 2,6-Diacetylpyridine, Palladium and Platinum complexes, Thiosemicarbazone.

*Corresponding author. Tel.: +34 914973868; fax: +34 914974833. E-mail address: ana.matesanz@uam.es

Abstract

Preparation and characterization of 2,6-diacetylpyridine bis(⁴*N-para*-chlorophenylthiosemicarbazone) ligand, H₂L, and its palladium(II) and platinum(II) complexes [PdL] and [PtL], is described. The ~~crystal and~~ molecular structure of the two new complexes has been determined by single crystal X-ray diffraction. The ligand act as dianionic tetradentate donor coordinating to the metal center in a square planar geometry through the **pyridine nitrogen** N_{pyridinic} atom and the **azomethine nitrogen** N_{iminic} and **thione sulfur** the S atoms from one thiosemicarbazone arm, the fourth coordination position is occupied by the **hydrazine nitrogen atom** N_{hydrazinic} of the other arm. New free ligand and its metal complexes have been evaluated for antiproliferative activity *in vitro* against NCI-H460, T-47D, A2780 and A2780cisR human cancer cell lines. The cytotoxicity data suggest that these compounds may be endowed with important antitumor properties, especially H₂L and [PtL] since they are capable of not only circumvent cisplatin resistance in A2780cisR cells but also exhibit high antiproliferative activity in breast cancer T-47D cells. The interaction of H₂L with calf thymus DNA was also investigated and its binding constant (K_b) determined.

1. Introduction

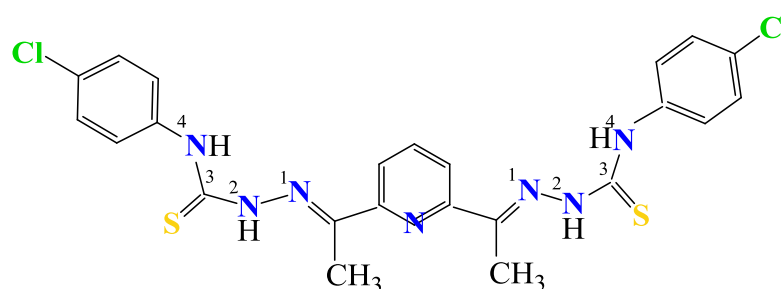
Platinum metallo-drugs are among the most effective agents for the treatment of cancer however its clinical utility is restricted due to the frequent development of drug resistance, the limited spectrum of tumors against which these drugs are active and also the severe normal tissue toxicity [1-5]. These disadvantages have driven the development of improved platinum-based anticancer drugs whose structure and mode of action differ from that of cisplatin, especially those that interact with specific molecular targets as for example are the processes associated to DNA: transcription, replication and repair [6-9].

In this regard, of particular interest are compounds targeting ribonucleotide reductase (RR), enzyme that catalyzes the reduction of ribonucleotides to deoxyribonucleotides and provides the building blocks for the de novo DNA synthesis in all living cells. Cancer cells require increased RR activity to meet the demand for deoxyribonucleotides that are needed to support their rapid proliferation. Thus inhibition of RR activity leads to inhibition of DNA synthesis and repair, and also induces cell cycle arrest and apoptosis [10-12].

α -(N)-heterocyclic thiosemicarbazones, (N)-TSCs, have been reported to be among the most effective RR inhibitors yet identified and many efforts have been devoted to the study of the structure–activity relationship of thiosemicarbazone derivatives. The anticancer activity of (N)-TSCs is closely related to the nature of the heterocyclic ring of the parent aldehyde or ketone, metal chelation ability and terminal amino substitution [13-20]. In this sense pyridine ring itself is a part of many natural and synthetically prepared pharmaceuticals and moreover it plays a significant role in many biological processes like nicotinamide adenine dinucleotide phosphate NADP or the important vitamins niacin and pyridoxine (vitamins B3 and B6) [21, 22].

Keeping in view the above observations and as part of our systematic investigation on the coordination chemistry of thiosemicarbazone derivatives we recently reported palladium(II) and platinum(II) complexes derived of 2,6-diacetylpyridine bis(⁴N- *ortho*-tolylthiosemicarbazone) and 2,6-diacetylpyridine bis(⁴N- *para*-tolylthiosemicarbazone) ligands. The *in vitro* antitumor studies have shown that these complexes exhibit important antiproliferative activity in A2780 and A2780cisR human cancer cell lines and these results encouraged us to further investigate their cytotoxic properties as well as those of novel derivatives [23].

This work is aimed to determine if the presence of an aryl ring with an electron withdrawing substituent (such as *para*-chlorophenyl group) results beneficial for the antitumor activity of 2,6-diacetylpyridine derived bis(⁴N-substituted thiosemicarbazones) **ligands derived from 2,6-diacetylpyridine**. Therefore here we describe the synthesis and chemical characterization of the new 2,6-diacetylpyridine bis(⁴N-*para*-chlorophenylthiosemicarbazone) ligand, H₂L, (Scheme 1) and its palladium(II) and platinum(II) complexes, [PdL] and [PtL].



Scheme 1. Structure of 2,6-diacetylpyridine bis(⁴N-*para*-chlorophenylthiosemicarbazone), H₂L ligand

The cytotoxic activity of the new compounds synthesized and cisplatin (assumed as the reference antitumor drug) against four human cancer cell lines: NCI-H460 (non-small cell lung cancer), T-47D (breast cancer), A2780 and A2780cisR (epithelial

epithelial ovarian cancer) has been studied. The interaction of H₂L with calf thymus DNA (CT-DNA) was also investigated and its binding constant (K_b) determined.

2. Experimental

2.1. Measurements

Elemental analyses were performed on a LECO CHNS-932 microanalyzer. Fast atom bombardment (FAB) mass spectra (MS) were performed on a VG AutoSpec spectrometer (~~m~~NBA: nitrobenzyl alcohol matrix). ¹H NMR spectra (~~DMSO-d₆~~) were recorded on Bruker AMX-300 spectrometer. All cited physical measurements were obtained out by the Servicio Interdepartamental de Investigación (SIIdI) of the Universidad Autónoma de Madrid.

Melting points were determined with a Stuart Scientific SMP3 apparatus. Infrared spectra (~~KBr pellets~~) were recorded on a Bomen–Michelson spectrophotometer (~~4000–400 cm⁻¹~~). ¹³C NMR spectra were recorded on a 400 Advance Bruker Fourier Transform spectrometer. Electronic spectra were recorded on a Thermo Scientific Evolution 260 Bio UV-visible (UV-VIS) spectrophotometer.

2.2. Materials

Solvents were purified and dried according to standard procedures. Hydrazine hydrate, 2,6-diacetylpyridine, *para*-chlorophenyl isothiocyanate, PdCl₂(PPh₃)₂ and PtCl₂(PPh₃)₂ were commercially available.

2.3. Synthesis of compounds

2,6-Diacetylpyridine bis(⁴*N*-~~para~~-chlorophenylthiosemicarbazone), H₂L. An ethanolic solution of hydrazine hydrate (0.250 g, 5 mmol) was added dropwise with constant stirring to an ethanolic solution of *para*-chlorophenyl isothiocyanate (0.848 g, 5 mmol). The reaction mixture was stirred for one more hour and then the white product

para-chlorophenylthiosemicarbazide formed was filtered, washed with cold ethanol and diethyl ether, dried *in vacuo* and recrystallized from ethanol. An ethanolic solution of the *para*-chlorophenylthiosemicarbazide (0.402 g, 2 mmol) was then stirred with 2,6-diacetylpyridine (0.163 g, 1 mmol) for 5 h. The resulting solution was reduced to half volume and the pale yellow solid formed was filtered, washed with ethanol, diethyl ether and finally dried *in vacuo*.

Yield (80%), mp 220 °C (decomposes). Elemental analysis found, C, 52.20; H, 4.25; N, 18.00; S, 12.20; C₂₃H₂₁N₇S₂Cl₂ requires C, 52.407; H, 4.003.99, N, 18.5048; S, 12.409 %. MS (FAB⁺ with *m*NBA: nitrobenzyl alcohol matrix) *m/z* 530.0 for [H₂L+H]⁺. IR (KBr pellet): ν_{max} /cm⁻¹ 3335, 3306, 3210 (w, NH); 1588 (s, CN); 827, 809 (w, CS-thioamide IV); 585 (pyridine ring). ¹H NMR (300 MHz, d⁶-DMSO, ppm), δ =10.80 [s, ²NH, 2H]; 10.20 [s, ⁴NH, 2H]; 8.55 [d, *J*=7.9 Hz, CH-pyridine, 2H]; 7.85 [t, *J*=7.9 Hz, CH-pyridine, 1H]; 7.60 (d, *J*=8.7 Hz, aromatic-thiosemicarbazide, 4H); 7.45 (d, *J*=8.7 Hz, aromatic-thiosemicarbazide, 4H); 2.50 (s, CH₃-diacetylpyridine, 6H). ¹³C NMR (d⁶-DMSO, ppm), δ =178.3 (C=S); 153.78 (C2,C6-pyridine); 149.85 (C=¹N); 138.54 (C4-pyridine); 137.17 (C3,C5-pyridine); 130.08 (aromatic-thiosemicarbazide); 128.49 (aromatic-thiosemicarbazide); 128.34 (aromatic-thiosemicarbazide); 127.37 (aromatic-thiosemicarbazide); 121.96 (aromatic-thiosemicarbazide); 12.98 (CH₃-diacetylpyridine). UV/VIS (DMSO): λ_{nm} 250, 337.

2,6-Diacetylpyridine bis(⁴N-*para*-chlorophenylthiosemicarbazonato)palladium(II), [PdL]. The reaction of H₂L ligand with PdCl₂(PPh₃)₂, in toluene, in presence of Et₃N, in 1:1 molar ratios over 20 h at room temperature led to the formation of an orange solution which was filtered and left to stand at ambient temperature for two days. The brown solid formed was filtered, washed several times with hot water, diethyl ether and finally dried *in vacuo*.

Yield (55%), mp >250 °C. Elemental analysis found, C, 43.35; H, 3.35, N, 15.10; S, 10.05; C₂₃H₁₉N₇S₂Cl₂Pd requires C, 43.50¹; H, 3.00², N, 15.40⁴; S, 10.10 %. MS (FAB⁺ with *m*NBA matrix) *m/z* 636 for [PdL¹+H]⁺. IR (KBr pellet): ν /cm⁻¹ 3243 (s, NH); 1595 (s, CN); 830, 804 (vw) (CS-thioamide IV); 603 (pyridine ring). ¹H NMR (300 MHz, d⁶-DMSO, ppm), δ =10.75, 10.18 [s, ⁴NH, 2H]; 8.43-8.10 [m, CH-pyridine, 3H]; 7.71-7.34 (m, aromatic-thiosemicarbazide, 8H); 2.72, 2.62 (s, CH₃-diacetylpyridine, 6H). UV/VIS (DMSO): λ /nm 267, 340, 410, 470.

Recrystallization from DMSO led to the isolation of orange crystals of [PdL]·DMSO that were suitable for X-ray-diffraction.

2,6-Diacetylpyridine bis(⁴N-*para*-chlorophenylthiosemicarbazonato)platinum(II), [PtL]. It was prepared by the same procedure as described for [PdL] by reaction of H₂L with PtCl₂(PPh₃)₂ and afforded a brown solid.

Yield (35%), mp 192 °C (decomposes). Elemental analysis found, C, 37.90; H, 2.55, N, 13.60; S, 8.60; C₂₃H₁₉N₇S₂Cl₂Pt requires C, 38.20¹⁸; H, 2.60⁵, N, 13.55; S, 8.85⁶ %. MS (FAB⁺ with *m*NBA matrix) *m/z* 724 for [PtL+H]⁺. IR (KBr pellet): ν /cm⁻¹ 3288, 3208 (s, NH); 1590 (s, CN); 826, 809 (vw) (CS-thioamide IV); 591 (pyridine ring). ¹H NMR (300 MHz, d⁶-DMSO, ppm), δ =11.00, 10.30 [s, ⁴NH, 2H]; δ =8.56-8.10 [m, CH-pyridine, 3H]; δ =7.76-7.70 (m, aromatic-thiosemicarbazide, 8H); δ =2.78, 2.71 (s, CH₃-diacetylpyridine, 6H). UV/VIS (DMSO): λ /nm 249, 267, 366.

Recrystallization from DMSO led to the isolation of orange crystals of [PtL]·DMSO that were suitable for X-ray-diffraction.

2.4. Crystallography

Data were collected on a Bruker X8 APEX II CCD. Crystallographic data and selected interatomic distances and angles are listed in Table 1. For all compounds, the software package SHELXTL was used for space group determination, structure

solution, and refinement [24]. The structures were solved by direct methods, completed with difference Fourier syntheses, and refined with anisotropic displacement parameters.

CCDC 981268 and 981269 contain the supplementary crystallographic data for compounds [PdL] and [PtL] respectively. These data can be obtained free of charge at www.ccdc.cam.ac.uk/conts/retrieving.html [or from the Cambridge Crystallographic Data Centre, 12, Union Road, Cambridge CB2 1EZ, UK; fax: +44-1223/336-033; e-mail: deposit@ccdc.cam.ac.uk].

2.5. *In vitro* antiproliferative activity

The human cancer cells: A2780 and A2780cisR (epithelial ovarian cancer), T-47D (breast cancer) and NCI-H460 (non-small cell lung cancer); were grown in RPMI-1640 medium supplemented with 10% foetal bovine serum (FBS) and 2 mM L-glutamine in an atmosphere of 5% CO₂ at 37 °C.

Cell proliferation was evaluated by the sulforhodamine B assay. Cells were plated in 96-well sterile plates at a density of $1.5 \cdot 10^4$ (for NCI-H460), $4 \cdot 10^3$ (for A2780 and A2780cisR) or $5 \cdot 10^3$ (for T-47D) cells per well with 100 µL of medium and were then incubated for 24 h (A2780, A2780cisR and NCI-H460) or 48 h (T-47D). After attachment to the culture surface the cells were incubated with various concentrations of the compounds tested freshly dissolved in DMSO (1 mg/mL) and diluted in the culture medium (DMSO final concentration 1%) for 48 h (for NCI-H460) or 96 h (for A2780, A2780cisR and T-47D). The cells were fixed by adding 50 µL of 30% trichloroacetic acid (TCA) per well.

The plates were incubated at 4 °C for 1 h and then washed five times with distilled water. The cellular material fixed with TCA was stained with 0.4% sulforhodamine B dissolved in 1% acetic acid for 10 min. Unbound dye was removed

by rinsing with 0.1% acetic acid. The protein-bound dye was extracted with 10 mM unbuffered Tris base for determination of optical density (at 515 nm) in a Tecan Ultra Evolution spectrophotometer.

The effects of compounds were expressed as corrected percentage inhibition values according to the following equation:

$$\% \text{ inhibition} = [1 - (T/C)] \times 100$$

where T is the mean absorbance of the treated cells and C the mean absorbance in the controls.

The inhibitory potential of compounds was measured by calculating concentration–percentage inhibition curves, these curves were adjusted to the following equation:

$$E = E_{\max} / [1 + (IC_{50}/C)^n]$$

where E is the percentage inhibition observed, E_{\max} is the maximal effects, IC_{50} is the concentration that inhibits 50% of maximal growth, C is the concentration of compounds tested and n is the slope of the semi-logarithmic dose–response sigmoid curves. This non-linear fitting was performed using GraphPad Prism software [25].

For comparison purposes, the antiproliferative activity of cisplatin was evaluated under the same experimental conditions. All compounds were tested in two independent studies with triplicate points. These experiments were carried out at the Unidad de Evaluación de Actividades Farmacológicas de Compuestos Químicos (USEF), Universidad de Santiago de Compostela.

2.6. DNA-Binding Experiments

CT-DNA stock solution was prepared by dissolving the lyophilized sodium salt in Tris-buffer (NaCl 50 mM, Tris-HCl 5 mM, pH was adjusted to 7.2 with NaOH 0.5

M) by stirring for 5 hours. The CT-DNA solution was standardized spectrophotometrically [26] by using its known molar absorption coefficient at 260 nm ($6600 \text{ M}^{-1} \cdot \text{cm}^{-1}$). The ratio of UV absorbance at 260 and 280 nm, A_{260}/A_{280} , of *ca.* 1.9, indicating that the DNA was sufficiently free of protein. Stock solution was kept frozen until the day of the experiment.

Concentrated stock solutions ($5 \cdot 10^{-3} \text{ M}$ and $5 \cdot 10^{-5}$) of H_2L were prepared dissolving the compound in DMSO. From these stock solutions, for all experiments the desired concentration of compound was achieved by dilution with Tris-buffer (NaCl 50 mM, Tris-HCl 5 mM, pH was adjusted to 7.2 with NaOH 0.5 M) to give homogeneous solutions with DMSO content of less than 2.5 %.

To investigate the binding mode, spectrophotometric titrations were performed at a fixed DNA concentration equal to $1.7 \cdot 10^{-4} \text{ M}$ with increasing concentration of H_2L (0-125 μM) compounds ($R = [\text{CT-DNA}]/[\text{compound}]$) and monitoring the absorbance change at the wavelength maximum 260 nm after incubation (10 min. at 37°C).

To calculate the binding parameters, the spectrophotometric titrations were performed with increasing concentration of DNA (0-40 μM) at a fixed compound concentration equal to 50 μM ($r = [\text{compound}]/[\text{DNA}]$) and monitoring the absorbance change in one characteristic charge transference band of the compound after incubation (10 min. at 37°C).

3. Results and discussion

3.1. Synthesis and spectroscopic characterization

A new 2,6-diacetylpyridine bis(4N -monosubstituted thiosemicarbazone) ligand has been synthesized with high purities and acceptable yields. The yellow compound

obtained is stable to air and moisture and was characterized by elemental analysis, FAB⁺ spectrometry and IR and ¹H NMR (¹H and ¹³C) spectroscopy.

Reaction of 2,6-diacetylpyridine bis(⁴N-~~para~~-chlorophenylthiosemicarbazone) ligand with equimolar amount of MCl₂(PPh₃)₂, where M = Pd(II) or Pt(II), led to the isolation of neutral mononuclear complexes [PdL] and [PtL] in which the bis(thiosemicarbazone) behaves as dianionic ligand with deprotonation of ~~hydrazine~~ ^{hydrazine} (²NH) protons and [NNNS] donor set.

Both complexes were characterized by routine analytical and spectroscopic techniques. Analytical data are consistent with the formulation given, thus in the FAB⁺ mass spectra ~~exhibited a very weak ion the molecular ion is seen as a small peak~~ at m/z = 636 for [PdL] and m/z = 724 for [PtL] ~~which corresponded to the predicted molecular weight of the [M+H]⁺ ions~~ and moreover the isotopic patterns of this signal fit well with the theoretical isotopic distributions.

The significant IR vibrational bands and the ¹H chemical shift values of the free ligand and its complexes are listed in the Experimental section and Scheme 1 shows the numbered structure of the free ligand. As the X-ray study has shown, during metal complexation, the ligand behaves as a tetradentate dianionic forming two five-membered and one six-membered chelate rings around the metal center. The high delocalization and the asymmetric coordination hinder the IR analysis. The stretching vibration $\nu(\text{C}=\text{N})$ and the in-plane pyridine deformation bands are slightly shifted to higher wavenumbers which are consistent with the implication of ~~imine~~ ^{imine} and ~~pyridine~~ ^{pyridine} nitrogen atoms in the coordination however this induces only minor changes in $\nu(\text{C}=\text{S})$ thioamide IV band which decreases slightly in intensity.

In the ¹H NMR spectrum of the double-armed H₂L ligand, two independent singlets at $\delta = 10.80$ and 10.20 ppm are observed for ~~²N-hydrazine and ⁴N-amide~~

~~hydrogens~~ $>\text{C}=\text{N}-^2\text{NH}-$ and $-\text{C}(\text{S})-^4\text{NH}-$ protons respectively. A doublet at $\delta = 8.55$ ppm and a triplet at $\delta = 7.85$ ppm are assigned to pyridyl ring protons. Aromatic ~~para~~-chlorophenyl protons appear as a multiplet at $\delta = 7.60-7.45$ ppm and a sharp singlet at $\delta = 2.50$ is assigned to the methyl protons. In [PdL] and [PtL] complexes, the anionic coordination of the ligand is evidenced by the disappearance of the signal corresponding to ^2N -hydrazinic ~~hydrogens~~ the $>\text{C}=\text{N}-^2\text{NH}-$ protons. On the other hand, ^4N -amide ~~hydrogens~~ the $-\text{C}(\text{S})-^4\text{NH}-$ protons appear two independent signals (10.75 and 10.218 ppm for [PdL] and 11.00 and 10.30 ppm for [PtL]) due to the asymmetric coordination. The pyridyl ring protons appear as a multiplet at $\delta = 8.43-8.10$ ppm for [PdL] and $\delta = 8.56-8.10$ ppm for [PtL] and the rest of the proton signals appear at nearly identical positions if they are compared with the corresponding ligand signals.

^{13}C NMR spectrum of the free ligand shows carbon signals supporting the ^1H NMR assignments however due to the low solubility of the complexes it was not possible to get ^{13}C NMR spectra of reasonably quality.

The electronic absorption spectra of both [H_2L] ligand and [PdL] and [PtL] complexes exhibit two intense band in the region 250-400 nm, which can ascribed to ligand-centered $n \rightarrow \pi^*$ and $\pi \rightarrow \pi^*$ transitions. In addition the spectra of metal complexes exhibit other less energetic bands assigned to a ligand to metal (LMCT) and metal to ligand charge transfer (MLCT) transitions [27].

3.2. Description of the crystal structures

[PdL]·DMSO and [PtL]·DMSO were isolated as neutral compounds. The most significant ~~parameters~~ crystallographic data for these complexes are shown in Tables 1, whereas selected bond lengths and bond angles are presented in Table and 2.

Table 1 Crystal data and structure refinement for **[PdL]·DMSO** and **[PtL]·DMSO** compounds.

	[PdL]·DMSO	[PtL]·DMSO
Molecular formula	C ₂₅ H ₂₅ Cl ₂ N ₇ OPdS ₃	C ₂₅ H ₂₅ Cl ₂ N ₇ OPtS ₃
Formula weight	713.00	801.69
Temperature (K)	100(2)	100(2)
Wavelength (Å)	0.71073	0.71073
Crystal system	Triclinic	Triclinic
Space group	<i>P</i> $\bar{1}$	<i>P</i> $\bar{1}$
a(Å)	7.4630(5)	7.484(3)
b(Å)	13.2509(7)	13.251(6)
c(Å)	14.6594(9)	14.680(6)
α /°	77.351(3)	76.611(14)
β /°	87.513(3)	87.296(15)
γ /°	81.522(3)	80.818(15)g
Volume(Å ³)	1398.96(15)	1398.0(10)
Z	2	2
Density (calculated) (g/cm ³)	1.693	1.905
Absorption coefficient (mm ⁻¹)	1.113	5.469
F(000)	720	784
Crystal size (mm ³)	0.57 x 0.09 x 0.03	0.40 x 0.04 x 0.02
Index ranges	-8≤h≤8, -15≤k≤15, -17≤l≤17	-8≤h≤8, -15≤k≤15, -16≤l≤17
Reflections collected	47797	15003
Independent reflections	5086	4672
Data / restraints / parameters	5086 /0/356	4672 /0/356
Goodness-of-fit on F ²	1.066	1.002
Final R indices [<i>I</i> >2σ(<i>I</i>)]	R1 = 0.0380, wR2 = 0.1116	R1 = 0.0450, wR2 = 0.1074
R indices (all data)	R1 = 0.0498, wR2 = 0.1297	R1 = 0.0748, wR2 = 0.1409
Largest diff. peak and hole, e.Å ⁻³	1.126 and -0.783	1.606 and -2.739

The structures together with the atom labeling schemes are shown in **Fig. Figures 1 and 2**. Both compounds are isostructural hence displaying nearly identical cell parameters, crystallize in the triclinic *P* $\bar{1}$ space group with Z=2 and the asymmetric units contain one molecule of the neutral complex and one dimethyl sulfoxide solvent molecule.

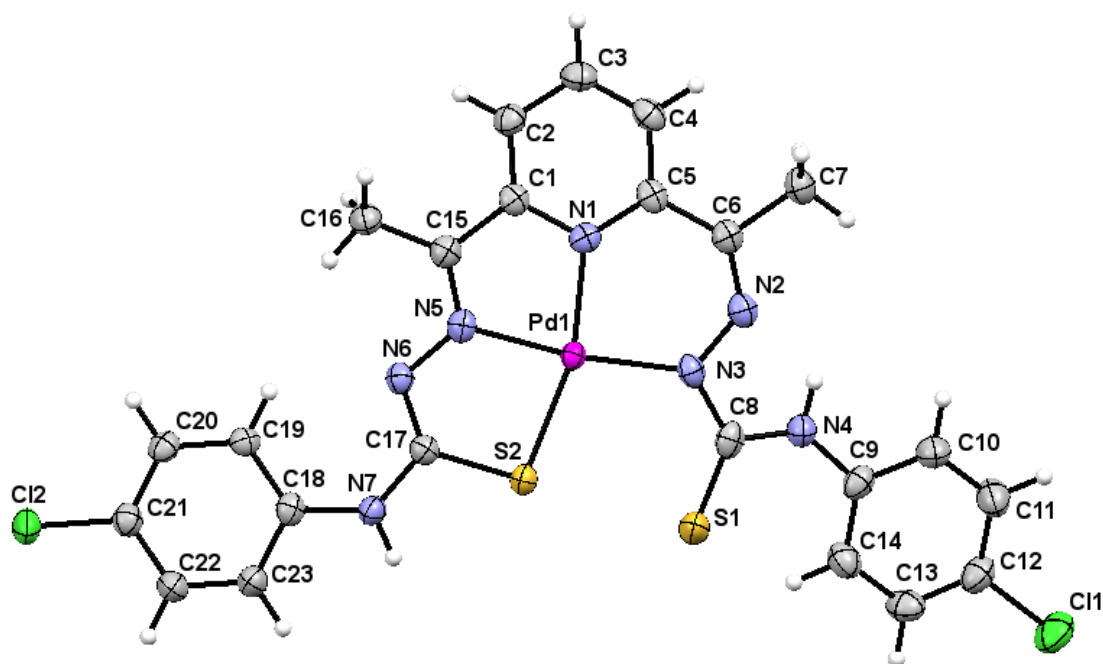


Fig. 1. Molecular structure of [PdL] complex. The displacement ellipsoids are drawn at the 50% probability.

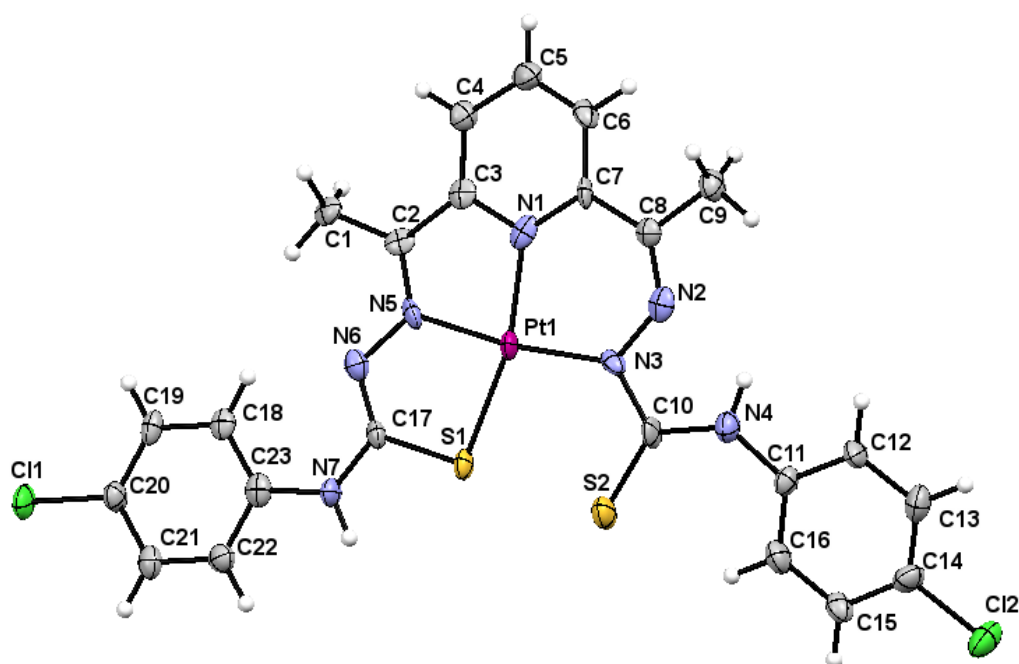


Fig. 2. Molecular structure of [PtL] complex. The displacement ellipsoids are drawn at the 50% probability.

The metal ion presents a square planar geometry being where the bis(thiosemicarbazone) ligand attached is coordinated to the metal ion through the

$N_{\text{pyridinic}}$ pyridine nitrogen atom and the N_{iminic} azomethine nitrogen and the S thione sulfur atoms from one thiosemicarbazone arm and being the fourth coordination position occupied by the $N_{\text{hydrazinic}}$ hydrazine nitrogen atom of the other thiosemicarbazone arm generating two typical five membered ($PdSCNN$ and $PdNCCN$ or $PtSCNN$ and $PtNCCN$) and one six membered ($PdNNCCN$ or $PtNNCCN$) chelate rings. Coordination by $N_{\text{hydrazinic}}$ hydrazine nitrogen atom instead of N_{iminic} the azomethine nitrogen atom, although uncommon, has been found in the bibliography for some d^8 bis(thiosemicarbazone) complexes [23, 28-31].

The $M-N$ and $M-S$ bond distances are similar to those found in other palladium(II) and platinum(II) complexes. It is important to note that the two thiosemicarbazone moieties, which are symmetrically deprotonated, coordinate in a different fashion. Upon coordination the bidentate- $N^{\wedge}S,S$ arm undergoes significant evolution from the thione to the thiol form which is reflected in $C-S$ distance of 1.779(4) for $[PdL]\cdot DMSO$ and 1.804(10) for $[PtL]\cdot DMSO$ while the monodentate- $N_{\text{hydrazinic}}$ thiosemicarbazone (3N , hydrazine nitrogen atom) arm maintains its thione form as reflects in their $C-S$ bond length of 1.673(5) for $[PdL]\cdot DMSO$ and 1.672(3) Å for $[PtL]\cdot DMSO$, typical of double $C=S$ bond.

Table 2. Selected bond distances (Å) and angles (°) for $[PdL]\cdot DMSO$ and $[PtL]\cdot DMSO$.

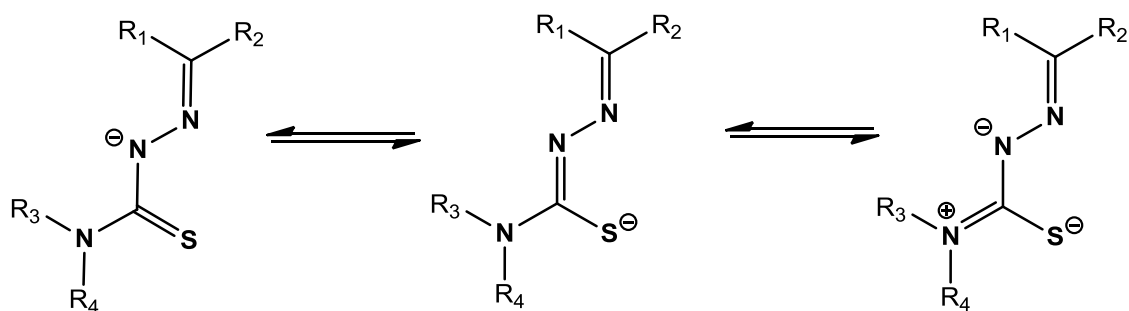
[PdL]•DMSO		[PtL]•DMSO	
Bond lengths (Å)			
S(1)-C(8)	1.673(5)	S(1)-C(17)	1.804(10)
S(2)-C(17)	1.779(4)	S(2)-C(10)	1.672(11)
C(6)-N(2)	1.291(6)	C(2)-N(5)	1.299(14)
C(8)-N(3)	1.389(6)	C(8)-N(2)	1.298(14)
C(8)-N(4)	1.373(6)	C(10)-N(3)	1.424(14)
C(9)-N(4)	1.406(6)	C(10)-N(4)	1.347(13)

C(15)-N(5)	1.304(6)	C(11)-N(4)	1.421(13)
C(17)-N(6)	1.297(6)	C(17)-N(6)	1.290(14)
C(17)-N(7)	1.367(6)	C(17)-N(7)	1.348(14)
C(18)-N(7)	1.402(6)	C(23)-N(7)	1.411(13)
Pd(1)-N(1)	2.029(4)	Pt(1)-N(1)	2.017(9)
Pd(1)-N(3)	2.044(4)	Pt(1)- N(3)	2.032(9)
Pd(1)-N(5)	1.979(4)	Pt(1)- N(5)	1.985(9)
Pd(1)-S(2)	2.2842(11)	Pt(1)-S(1)	2.279(3)

Bond angles (°)

N(1)-Pd(1)-N(3)	91.73(15)	N(1)-Pt(1)-N(3)	91.8(3)
N(1)-Pd(1)-N(5)	80.58(15)	N(1)-Pt(1)-N(5)	80.5(4)
N(3)-Pd(1)-S(2)	104.2(11)	N(3)-Pt(1)-S(2)	103.7(2)
N(5)-Pd(1)-S(2)	83.43(11)	N(5)-Pt(1)-S(2)	83.0(3)
N(1)-Pd(1)-S(2)	163.95(11)	N(1)-Pt(1)-S(2)	164.5(3)
N(3)-Pd(1)-N(5)	172.25(15)	N(3)-Pt(1)-N(5)	172.2(4)

Comparison of C–N and N–N bond distances with typical lengths of single and double bonds [C–N 1.47, C=N 1.28 Å, N–N 1.45, N=N 1.25 Å] suggests extensive charge delocalization over the thiosemicarbazone moieties [32, 33] and also agree with the thiolate tautomeric form of the bidentate thiosemicarbazionate arm and the thione tautomeric form of the monodentate one (Scheme 2).



Scheme 2. Delocalization System in the Thiosemicarbazionate moiety

Inspection of the angles formed between the metal ion ($M = Pd^{2+}, Pt^{2+}$) and the coordinated atoms shows that the metal is contained within a slightly distorted square-planar environment being the bond angles between adjacent coordinating atoms in the range 80.5-104.2° range.

The crystal structures are stabilized by intermolecular hydrogen interactions involving the N(7) atom of the bidentate thiosemicarbazone arms and the oxygen atom of DMSO solvent molecule being the N(7)-H(7)···O(1) contact distance 2.83 Å for both complexes and $\angle(NHO)$ angle 170.4° for [PdL] and 169.2° for [PtL]. Further stabilization of the crystal packing is provided by intermolecular π - π stacking interactions involving the whole planar bis(thiosemicarbazone)-metal skeleton (Figure 3), with an interplane separation of about ≈ 3.5 Å.

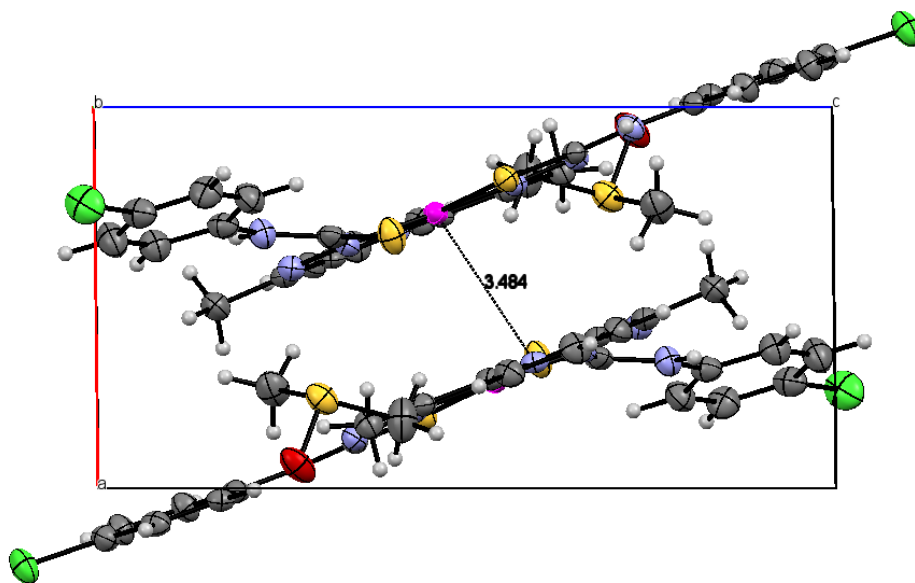


Fig 3. Crystal packing view of [PdL]·DMSO along a axis, dashed lines denote π ··· π interactions.

3.3. In vitro antiproliferative activity

To assess the antitumor potential of the synthesized compounds, its antiproliferative activity (in powder solid form) was tested *in vitro* against a panel of

human cancer cells lines containing examples of lung (NCI-H460), breast (T-47D,) and ovarian (A2780 and A2780cisR) cancers. For comparison purposes, the cytotoxicity of cisplatin was always evaluated under the same experimental conditions.

Table 3 shows that both the *p*-chlorophenyl substituted free ligand H₂L and its platinum(II) complex [PtL] present important antiproliferative activity in the low-micromolar range, against ovarian (A2780, cisplatin sensitive, and A2780cisR, cisplatin resistant) and breast (T-47D) cancer cells. It is remarkable to note that both compounds exhibit better cytotoxic effects against T-47D cells than cisplatin by comparing their IC₅₀ values.

The A2780cisR cell line encompasses all of the known major mechanisms of resistance to cisplatin: reduced drug transport, enhanced DNA repair/tolerance, and elevated GSH levels. The ability of H₂L and [PtL] compounds to circumvent cisplatin-acquired resistance was confirmed from the resistance factor values, RF (defined as IC₅₀ in A2780cisR/IC₅₀ in A2780) since both have a much better RF than cisplatin. An RF value of < 2 was considered to denote non-cross-resistance and therefore these compounds are able to circumvent cisplatin resistance [34,35].

From a chemical point of view, analysis of these data together with those of our previous study [23] in which the related ligand 2,6-diacetylpyridine bis(⁴*N*-para-tolylthiosemicarbazone), H₂L², resulted inactive in both A2780 and A2780cisR cell lines and its [PtL²] complex showed a slightly lower antiproliferative activity than [PtL] complex (see table 3) [23] suggests that the presence of one electron withdrawing group attached to the ⁴N atom of the thiosemicarbazone moiety results beneficial for the antiproliferative activity of the bis(thiosemicarbazone) ligands of the 2,6-diacetylpyridine series.

Table 3. *In vitro* antiproliferative activity of bis(thiosemicarbazone) compounds **H₂L**, **[PdL]** and **[PtL]** complexes and **H₂L²**, **[PtL²]** and cisplatin, evaluated in human T-47D (breast cancer), A2780 and A2780cisR (epithelial ovarian cancer) cell lines.

IC ₅₀ ±SD (μM)				
	A2780	A2780cisR	T-47D	RF IC ₅₀ (A2780cisR)/IC ₅₀ (A2780)
H₂L	7.16±0.14	13±1	7.42±0.14	1.8
[PdL]	24±1	>100	>100	> 4.2
[PtL]	7.12±0.21	9.13±0.07	9.17±0.07	1.3
H₂L²	>100 ^a	>100 ^a	ND	---
[PtL²]	20±2 ^a	18±1 ^a	ND	1.1
Cisplatin	0.88±0.01	7.77±0.10	12±1	8.8

The IC₅₀ values are averages of two independent determinations.

ND = not determined

^a Values taken from Ref. [23]

3.4. DNA Interaction Studies

In order to initially address if any direct interaction with DNA is part of the mechanism of action of the compounds, UV-visible absorption spectra in absence and presence of calf thymus DNA (CT-DNA) were carried out for H₂L ligand, which have a significant effect against the tested cell lines.

Absorption spectral studies

The binding affinity between DNA and H₂L ligand can be detected by UV-Vis absorption spectroscopy by measuring the changes in the absorption properties of: a)

DNA (for a variable H₂L concentration) or b) H₂L ligand molecule (for a variable DNA concentration).

The UV-Vis absorption spectrum of the typical B β -form DNA exhibits a characteristic $\pi \rightarrow \pi^*$ band at 260 nm as consequence of the chromophoric groups in purine and pyrimidine moieties. Compounds binding with DNA through intercalation are consistent with hypochromism (decrease in DNA band absorption), resulted of a stacking interaction between the aromatic ligand chromophore and the base pair of DNA. In case of compounds binding with DNA through external contact (including groove binding and electrostatic attraction) usually hyperchromism (increase in DNA band absorption) is observed which is attributable of a contraction and overall damage of the secondary structure of DNA [36].

Thus, the absorption spectrum of CT-DNA in presence of H₂L was recorded, by keeping constant CT-DNA concentration ($1.7 \cdot 10^{-4}$ M) in diverse [CT-DNA]/[H₂L] mixing ratios ($R = 0.5-1.5$) and monitoring the change in the absorption intensity of the typical CT-DNA spectral band at 260 nm. As Figure 4 shows, when the concentration of H₂L is gradually increased a significant increase in absorption of the DNA band occurs being the percentage of hyperchromism observed [% hyperchromism = $(A_{\text{DNA bound}} - A_{\text{DNA free}}) / A_{\text{DNA bound}}$] about 40 %.

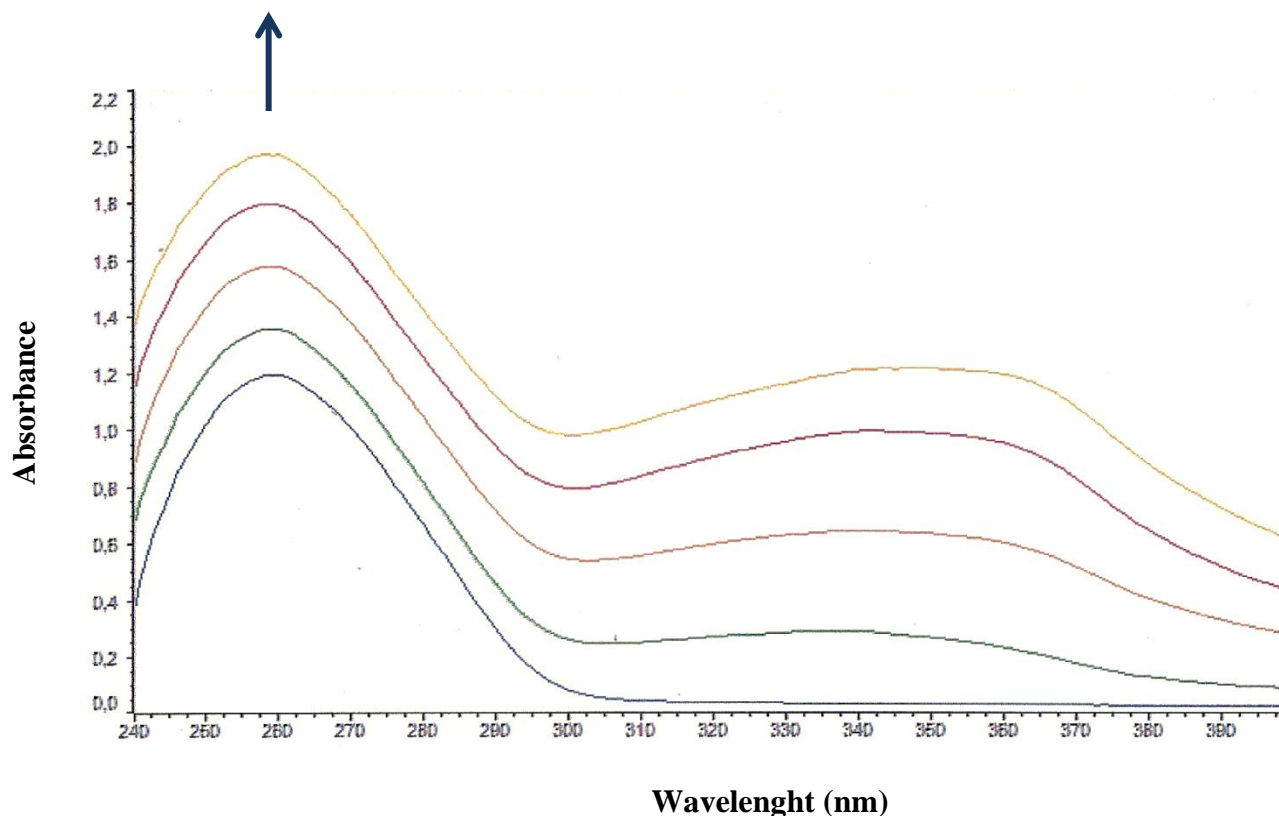


Fig. 4. UV absorption spectrum of CT-DNA in the absence (black curve) and presence of increasing amounts of compound H_2L . The data were collected for $[CT-DNA] = 1.7 \cdot 10^{-4}$ M and $[H_2L] = 0, 2.5 \cdot 10^{-6}, 6.0 \cdot 10^{-5}, 8.0 \cdot 10^{-5}, 1.25 \cdot 10^{-4}$ M ~~$[CT-DNA]/[H_2L]$ -mixing ratios $R = 0.5-1.5$~~ (the arrow shows the changes upon increasing amounts of complex).

These characteristics suggest non-covalent surface (major or minor groove) binding along outside of DNA helix. The above observations are comparable to those reported earlier for various neutral bis(thiosemicarbazone) palladium and platinum complexes [37, 38].

The H_2L ligand exhibit, in DMSO:Tris buffer (2.5:100) mixture, one broad intense band of intraligand $\pi-\pi^*$ transition at 250 nm and other less intense of intraligand $n-\pi^*$ transition at 337 nm and any interaction with DNA could perturb it.

~~So~~ **Thus**, in order to determine the intrinsic binding constant (K_b), absorption titration experiments were performed by maintaining a constant H_2L concentration (50 μM) while gradually increasing the concentration of DNA (0 - 40 μM) and monitoring the change in the absorption intensity of the intraligand charge transfer band. While measuring the absorption spectra, an equal amount of DNA was added to both the test

solution and the reference solution to eliminate the absorbance of DNA itself. The data were then fitted to the following equation, that is only valid for low compound:DNA ratios (i.e., far from the DNA saturation) and assumes no binding cooperativity [39]:

$$[\text{DNA}] / (\varepsilon_a - \varepsilon_f) = [\text{DNA}] / (\varepsilon_b - \varepsilon_f) + 1 / \{K_b (\varepsilon_b - \varepsilon_f)\}$$

where $[\text{DNA}]$ is the concentration of the nucleic acid in base pairs, ε_a is the apparent absorption coefficient obtained by calculating $A_{\text{obs}}/[\text{compound}]$, and ε_f and ε_b are the absorption coefficients of the free and the fully bound compound, respectively.

A plot (Figure 5) of $[\text{DNA}]/(\varepsilon_b - \varepsilon_f)$ versus $[\text{DNA}]$, gives a slope of $1/(\varepsilon_b - \varepsilon_f)$ and a Y-intercept equal to $1/\{K_b(\varepsilon_b - \varepsilon_f)\}$. The intrinsic binding constant K_b is calculated as the ratio of the slope to the Y-intercept.

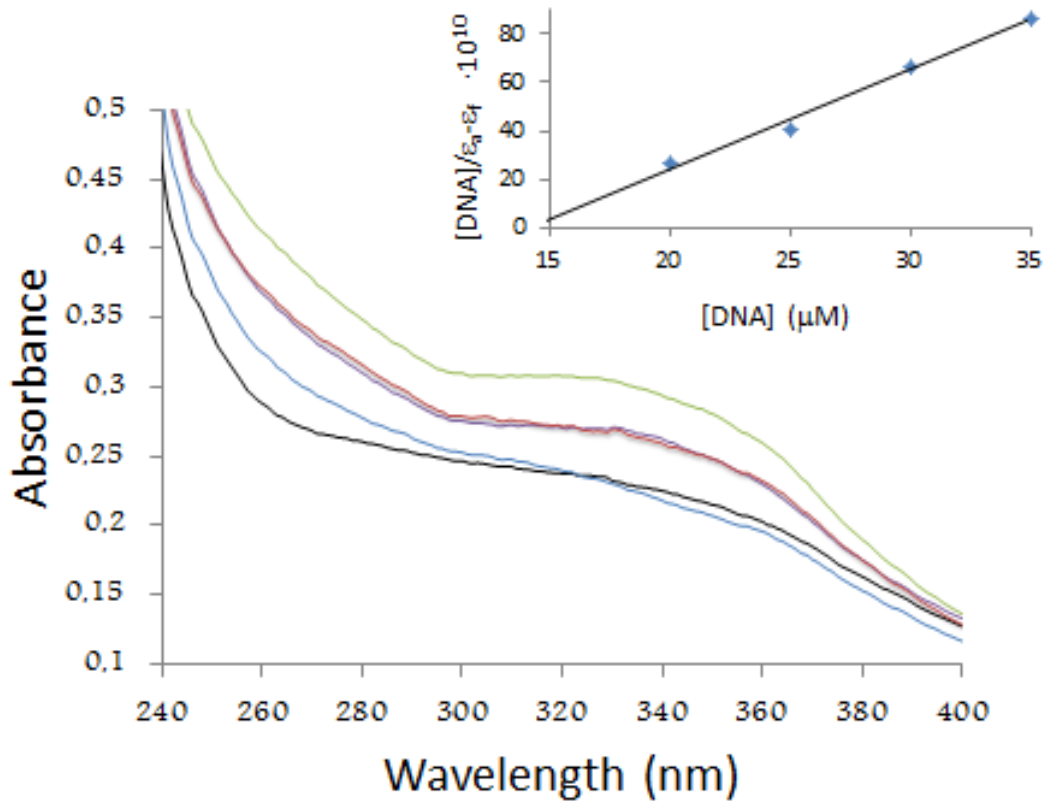


Fig. 5. UV absorption spectrum of H_2L in the absence (black curve) and presence of increasing amounts of compound CT-DNA. The data were collected for $[\text{H}_2\text{L}] = 5 \cdot 10^{-5} \text{ M}$ and

$[CT-DNA] = 0, 20 \cdot 10^{-6}, 60 \cdot 10^{-6}, 70 \cdot 10^{-6}, 75 \cdot 10^{-6} \text{ M}$ $[H_2L]/[CT-DNA]$ mixing ratios $r = 0.4-0.7$. The insert shows a fitting of the absorbance data used to obtain the binding constants.

On titration of CT-DNA a slight increase in the absorptivity of this band is observed which is indicative of interaction between the electronic states of the ligand chromophore with that of DNA bases. The magnitude of intrinsic binding constant was calculated to be $7.03 \cdot 10^2 \text{ M}^{-1}$ (correlation coefficient $R^2 = 0.99$) which is modest, however it should be kept in mind that the biological activity of α -(N)-heterocyclic thiosemicarbazones is not only due to their non-covalent DNA binding but they are also potent inhibitors of DNA synthesis and repair through RR inactivation. This fact could explain the good cytotoxic activity that both free ligand and platinum complex have demonstrated. Further studies and more practical experiments are required to elucidate the biochemical mechanisms involved in their activity.

4. Conclusions

A new family of Pt(II) and Pd(II) bis(thiosemicarbazone) compounds of the 2,6-diacetylpyridine series containing an aryl ring with an electron withdrawing substituent (~~para~~-chlorophenyl group) has been successfully prepared and characterized.

This study has identified both the free ligand H_2L and the Pt(II) complex $[PtL]$ as having high antiproliferative activity since they are capable of not only circumvent cisplatin resistance in A2780cisR cells but they also exhibit high antiproliferative activity against breast (T-47D) cancer cells.

Acknowledgments

We are grateful to Ministerio de Economía y Competitividad, Instituto de Salud Carlos III of Spain (PI1100659) for financial support.

References

- [1] N.J. Wheate, S. Walker, G.E. Craig, R. Oun, Dalton Trans. 39 (2010) 8113-8127.
- [2] E. Wong, C.M. Giandomenico, Chem. Rev. 99 (1999) 2451-2466.
- [3] Z. Guo, P.J Sadler, Angew. Chem. Int. Ed. 38 (1999) 1512-1531.
- [4] M.S. Razzaque, Nephrol. Dial. Transplant. (2007) 1-5.
- [5] M. Okuda, K. Masaki, S. Fukatsu, Y. Hashimoto, K. Inui, Biochem. Pharmacol. 59 (2000) 195–201.
- [6] K. van der Schilden, F. García, H. Kooijman, A.L. Spek, J.G. Haasnoot, J. Reedijk, Angew. Chem. Int. Ed. 43 (2004) 5668-5670.
- [7] L.H. Hurley, Nature Reviews Cancer, 2 (2002) 188-200.
- [8] T.W. Hambley, Coord. Chem. Rev. 166 (1997) 181-223.
- [9] J. Kasparkova, V. Marini, Y. Najajreh, D. Gibson, V. Brabec, Biochemistry 42 (2003) 6321-6332.
- [10] J. Shao, X. Liu, L. Zhu, Y. Yen, Expert. Opin. Ther. Targets 17 (2013) 1423-1437.
- [11] D.S. Kalinowski, D.R. Richardson, *Pharmacol. Rev.* 57 (2005) 547–583.
- [12] C. Kunos, T. Radivoyevitch, F.W. Abdul-Karim, J. Fanning, O. Abulafia, A.J. Bonebrake, L. Usha, J. Transl. Med. (2012) 10:79.
- [13] L. Zhu, B. Zhou, X. Chen, H. Jiang, J. Shao, Y. Yen, *Biochem Pharmacol.* 78 (2009) 1178-1185.
- [14] M. Liu, T. Lin, A.C. Sartorelli, *Prog. Med. Chem.* 32 (1995) 1-35.
- [15] D.X. West, A.E. Liberta, S.B. Padhye, R.C. Chikate, P.B. Sonawane, A.S. Kumbhar, R.G. Yerande, *Coord. Chem. Rev.* 123 (1993) 49.
- [16] A.I. Matesanz, P. Souza, *Mini-rev. Med. Chem.* 9 (2009) 1389-89.
- [17] C.R. Kowol, R. Berger, R. Eichinger, A. Roller, M.A. Jakupec, P. Schmidt, V.B. Arion, B.K. Keppler, *J. Med. Chem.* 50 (2007) 1254-1265.

- [18] R. A. Finch, M. C. Liu, A. H. Cory, J. G. Cory and A. C. Sartorelli, *Adv. Enzyme Regul.* 39 (1999) 3–12.
- [19] P. Heffeter, C. Pirker, C.R. Kowol, G. Herrman, R. Dornetshuber, W. Miklos, U. Jungwirth, G. Koellensperger, B.K. Keppler, W. Berger, *Biochem. Pharmacol.* 83 (2012) 1623-1633.
- [20] E. Ramachandran, D.S. Raja, J.L. Mike, T.R. Wagner, M. Zellerb, K. Natarajan, *RSC Adv.* 2 (2012) 8515–8525.
- [21] E. Lukevits, *Chem. Heterocyc. Comp.* 31 (1995) 639–650.
- [22] L.E. Kapinos, H. Sigel, *Inorg. Chim. Acta* 337 (2002) 131-142.
- [23] A.I. Matesanz, I. Leitao, P. Souza, J. Inorg. Biochem. 125 (2013) 26–31.
- [24] SHELXTL-NT version 6.12, Structure Determination Package, Bruker-Nonius AXS, Madison, Wisconsin, USA, 2001.
- [25] GraphPad Prism, version 2.01, GraphPad Software, Inc., San Diego, CA, 1996.
- [26] M.A. Ali, A.H. Mirza, A.L. Tan, L.K. Wei, P.V. Bernhardt, *Polyhedron* 23 (2004) 2037–2043.
- [27] A.A. Ali, H. Nimir, C. Aktas, V. Huch, U. Rauch, K. Schäfer, M. Veith, *Organometallics*, 31 (2012) 2256–2262.
- [28] A.I. Matesanz, P. Souza, *Inorg. Chem. Commun.* 27 (2013) 5–8.
- [29] C.A. Brown, W. Kaminsky, K.A. Claborn, K.I. Goldberg, D.X. West, J. Braz. Chem.Soc. 13 (2002) 10–18.
- [30] J.I. Gradinaru, S.T. Malinowski, M.A. Popovici, M. Gdaniec, *Crystallogr. Rep.* 50 (2005) 217–223.
- [31] T.R. Todorović, A. Bacchi, G. Pelizzi, N.O. Juranić, D.M. Sladić, I.D. Brčeski, K.K. Anelković, *Inorg. Chem. Commun.* 9 (2006) 862–865.
- [32] R. Pedrido, A.M. González-Noya, M.J. Romero, M. Martínez-Calvo, M. Vázquez

- López, E. Gómez-Fórneas, G. Zaragoza, M.R. Bermejo, Dalton Trans. (2008) 6776–6787.
- [33] J.S. Casas, M.S. García-Tasende, J. Sordo, Coord. Chem. Rev. 209 (2000) 197–261.
- [34] L.R. Kelland, C.F.J. Barnard, K.J. Mellish, M. Jones, P.M. Goddard, M. Valenti, A. Bryant, B.A. Murrer, K.R. Harrap, Cancer Res. 54 (1994) 5618–5622.
- [35] J. Ruiz, C. Vicente, C. Haro, D. Bautista, Inorg. Chem. 52 (2013) 974–982.
- [36] F. Arjmand and M. Aziz, Eur. J. Med. Chem., 2009, 44, 834–844.
- [37] A.I. Matesanz, C. Hernández, A. Rodríguez, P. Souza, Dalton Trans. 40 (2011) 5738–5745.
- [38] A.I. Matesanz, J. Perles, P. Souza, Dalton Trans. 41 (2012) 12538–12547.
- [39] B. Pedras, R.M.F. Batista, L. Tormo, S.P.G. Costa, M.M.M. Raposo, G. Orellana, J.L. Capelo, C. Lodeiro, Inorg. Chim. Acta, 381 (2012) 95–103.

Table 1 Crystal data and structure refinement for [PdL]·DMSO and [PtL]·DMSO.

	[PdL]·DMSO	[PtL]·DMSO
Molecular formula	C ₂₅ H ₂₅ Cl ₂ N ₇ OPdS ₃	C ₂₅ H ₂₅ Cl ₂ N ₇ OPtS ₃
Formula weight	713.00	801.69
Temperature (K)	100(2)	100(2)
Wavelength (Å)	0.71073	0.71073
Crystal system	Triclinic	Triclinic
Space group	<i>P</i> $\bar{1}$	<i>P</i> $\bar{1}$
a(Å)	7.4630(5)	7.484(3)
b(Å)	13.2509(7)	13.251(6)
c(Å)	14.6594(9)	14.680(6)
α /°	77.351(3)	76.611(14)
β /°	87.513(3)	87.296(15)
γ /°	81.522(3)	80.818(15)g
Volume(Å ³)	1398.96(15)	1398.0(10)
Z	2	2
Density (calculated) (g/cm ³)	1.693	1.905
Absorption coefficient (mm ⁻¹)	1.113	5.469
F(000)	720	784
Crystal size (mm ³)	0.57 x 0.09 x 0.03	0.40 x 0.04 x 0.02
Index ranges	-8≤h≤8, -15≤k≤15, -17≤l≤17	-8≤h≤8, -15≤k≤15, -16≤l≤17
Reflections collected	47797	15003

Independent reflections	5086	4672
Data / restraints / parameters	5086 /0/356	4672 /0/356
Goodness-of-fit on F ²	1.066	1.002
Final R indices [$I > 2\sigma(I)$]	R1 = 0.0380, wR2 = 0.1116	R1 = 0.0450, wR2 = 0.1074
R indices (all data)	R1 = 0.0498, wR2 = 0.1297	R1 = 0.0748, wR2 = 0.1409
Largest diff. peak and hole, e.Å ⁻³	1.126 and -0.783	1.606 and -2.739

Table 2

Table 2. Selected bond distances (Å) and angles (°) for [PdL]·DMSO and [PtL]·DMSO.

[PdL]·DMSO		[PtL]·DMSO	
Bond lengths (Å)			
S(1)-C(8)	1.673(5)	S(1)-C(17)	1.804(10)
S(2)-C(17)	1.779(4)	S(2)-C(10)	1.672(11)
C(6)-N(2)	1.291(6)	C(2)-N(5)	1.299(14)
C(8)-N(3)	1.389(6)	C(8)-N(2)	1.298(14)
C(8)-N(4)	1.373(6)	C(10)-N(3)	1.424(14)
C(9)-N(4)	1.406(6)	C(10)-N(4)	1.347(13)
C(15)-N(5)	1.304(6)	C(11)-N(4)	1.421(13)
C(17)-N(6)	1.297(6)	C(17)-N(6)	1.290(14)
C(17)-N(7)	1.367(6)	C(17)-N(7)	1.348(14)
C(18)-N(7)	1.402(6)	C(23)-N(7)	1.411(13)
Pd(1)-N(1)	2.029(4)	Pt(1)-N(1)	2.017(9)
Pd(1)-N(3)	2.044(4)	Pt(1)- N(3)	2.032(9)
Pd(1)-N(5)	1.979(4)	Pt(1)- N(5)	1.985(9)
Pd(1)-S(2)	2.2842(11)	Pt(1)-S(1)	2.279(3)
Bond angles (°)			
N(1)-Pd(1)-N(3)	91.73(15)	N(1)-Pt(1)-N(3)	91.8(3)
N(1)-Pd(1)-N(5)	80.58(15)	N(1)-Pt(1)-N(5)	80.5(4)
N(3)-Pd(1)-S(2)	104.2(11)	N(3)-Pt(1)-S(2)	103.7(2)

N(5)-Pd(1)-S(2)	83.43(11)	N(5)-Pt(1)-S(2)	83.0(3)
N(1)-Pd(1)-S(2)	163.95(11)	N(1)-Pt(1)-S(2)	164.5(3)
N(3)-Pd(1)-N(5)	172.25(15)	N(3)-Pt(1)-N(5)	172.2(4)

Table 3

Table 3. *In vitro* antiproliferative activity of H₂L, [PdL] and [PtL] complexes and H₂L², [PtL²] and cisplatin, evaluated in human T-47D ([breast cancer](#)), A2780 and A2780cisR (epithelial ovarian cancer) cell lines.

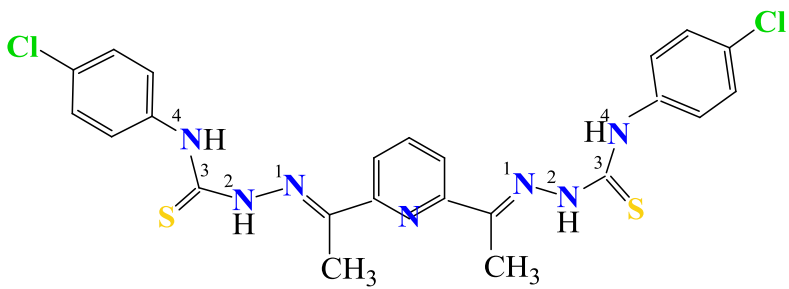
IC ₅₀ ±SD (µM)				
	A2780	A2780cisR	T-47D	RF IC ₅₀ (A2780cisR)/IC ₅₀ (A2780)
H ₂ L	7.16±0.14	13±1	7.42±0.14	1.8
[PdL]	24±1	>100	>100	> 4.2
[PtL]	7.12±0.21	9.13±0.07	9.17±0.07	1.3
H ₂ L ²	>100 ^a	>100 ^a	ND	---
[PtL ²]	20±2 ^a	18±1 ^a	ND	1.1
Cisplatin	0.88±0.01	7.77±0.10	12±1	8.8

The IC₅₀ values are averages of two independent determinations.

ND = not determined

^a Values taken from Ref. [23]

Scheme 1



Scheme 2

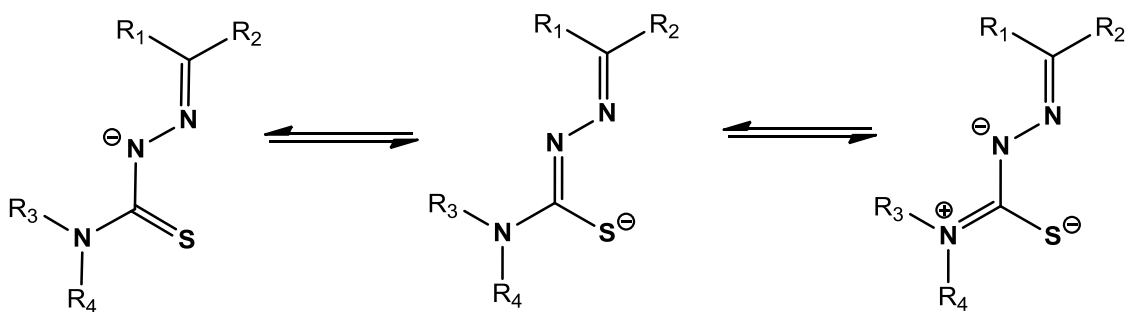


Figure 1

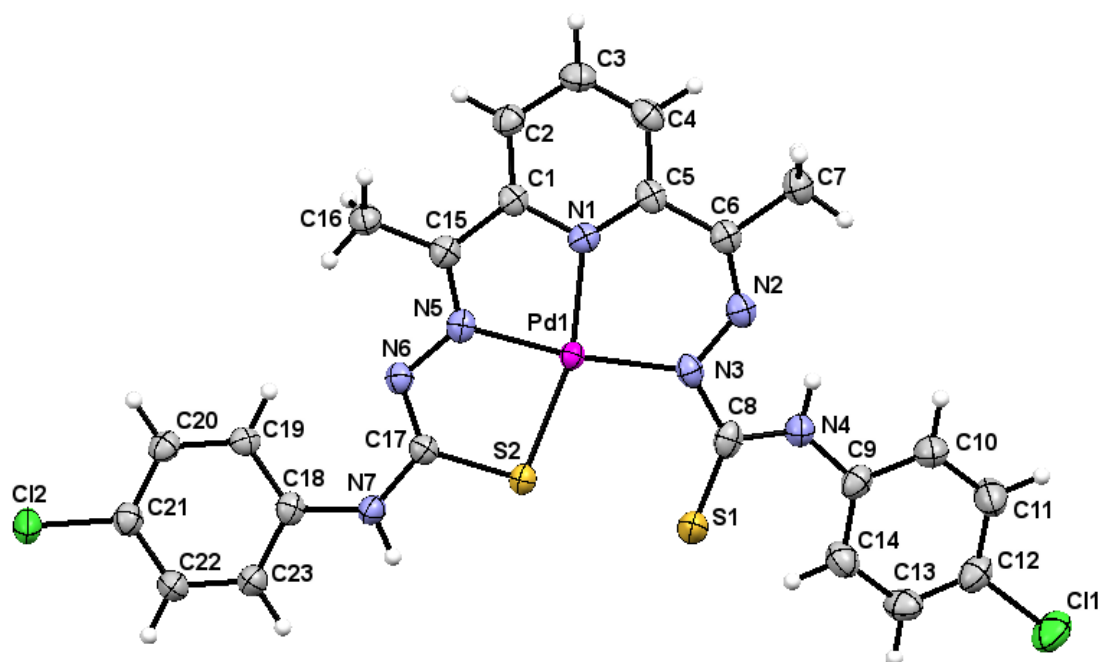


Figure 2

[Click here to download Figure\(s\): Figure 2.docx](#)

Figure 2

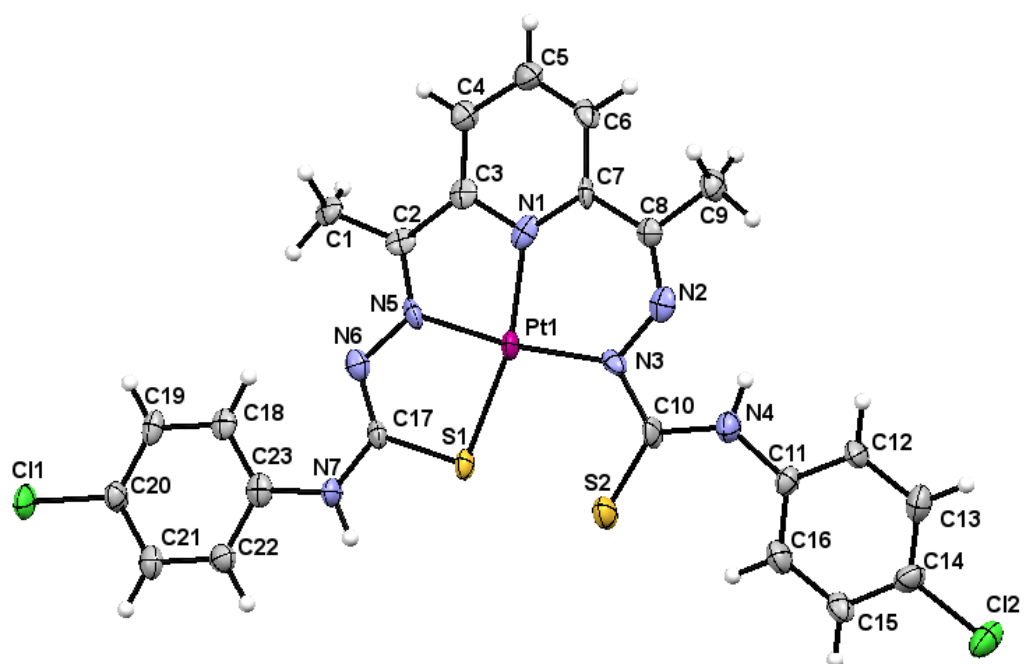


Figure 3

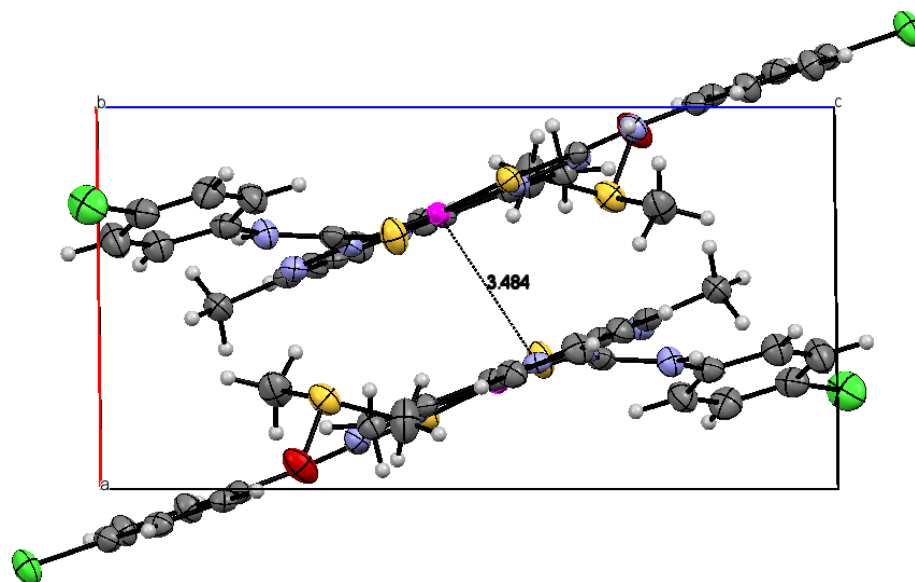


Figure 4

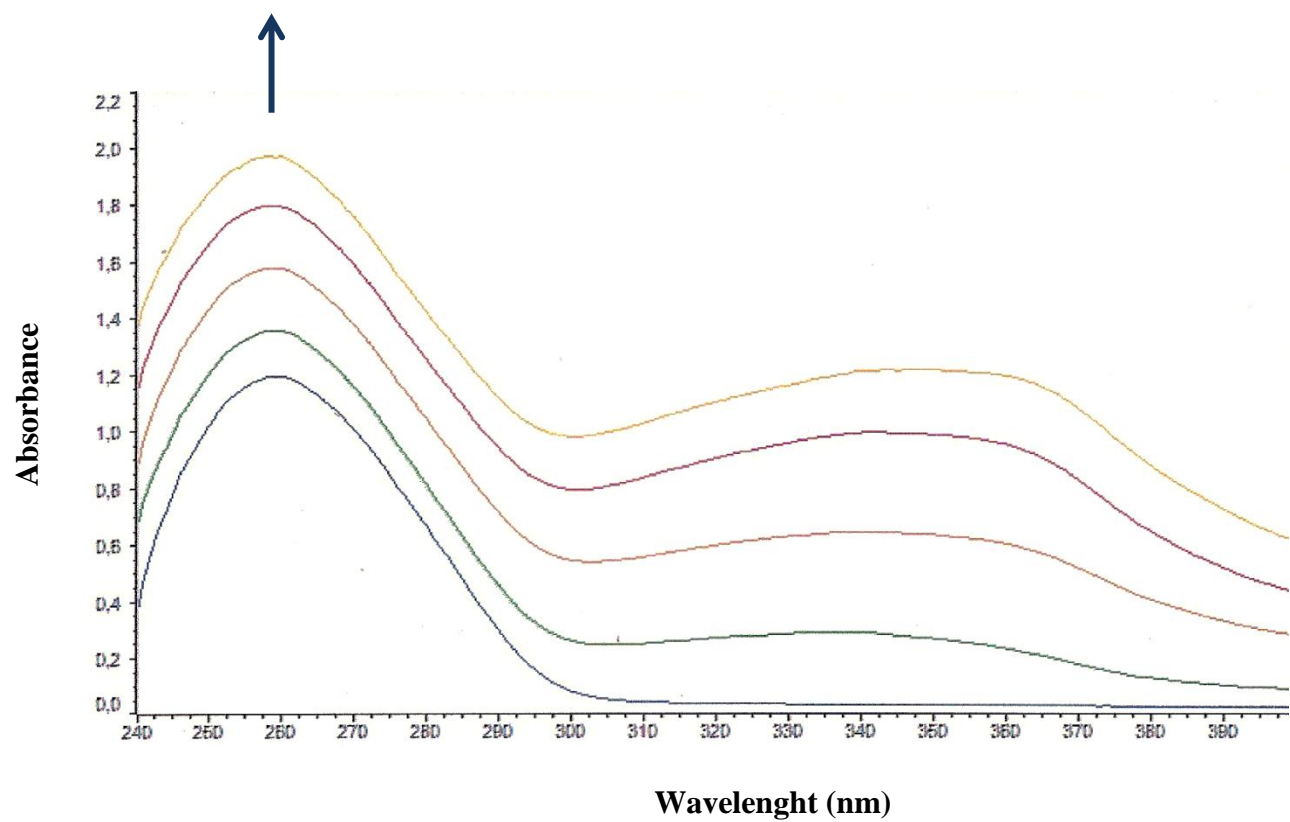


Figure 5

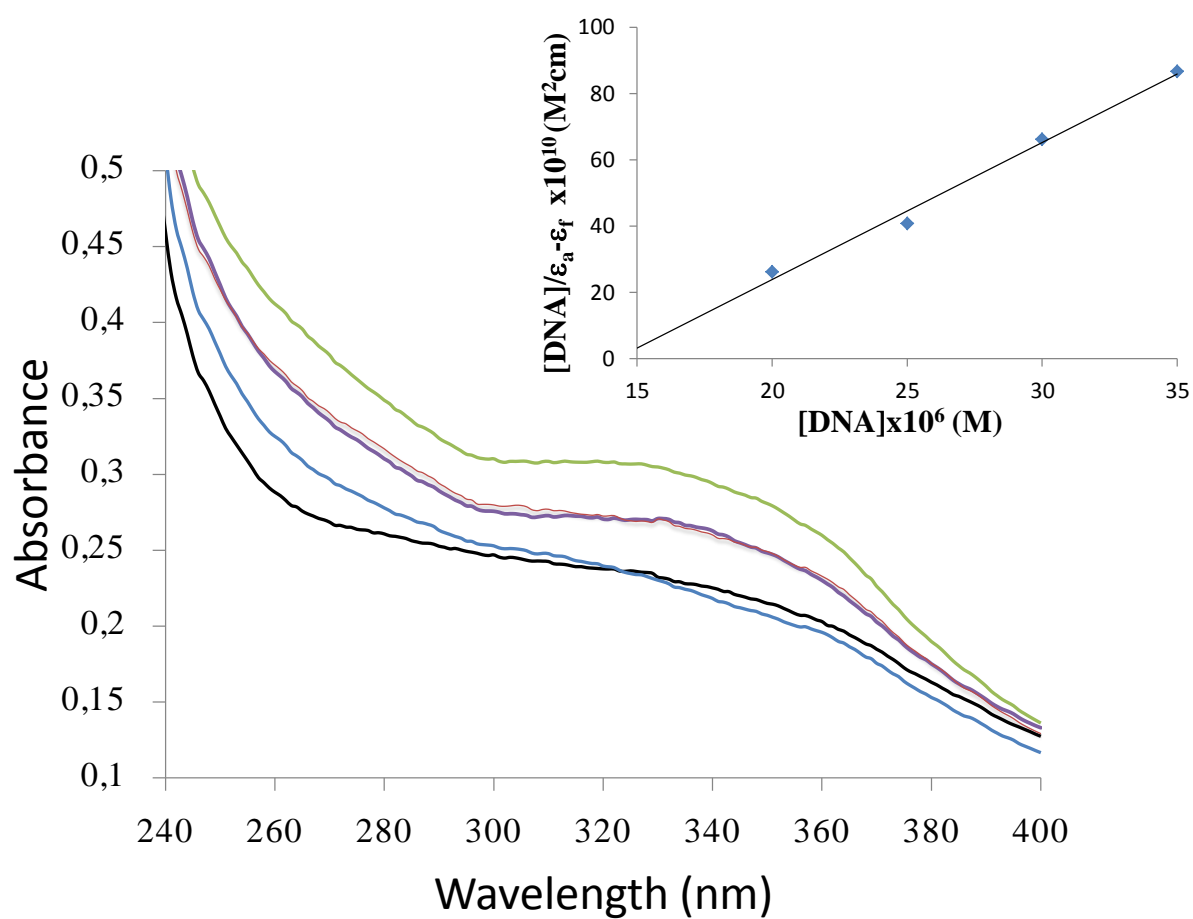


Figure S1.

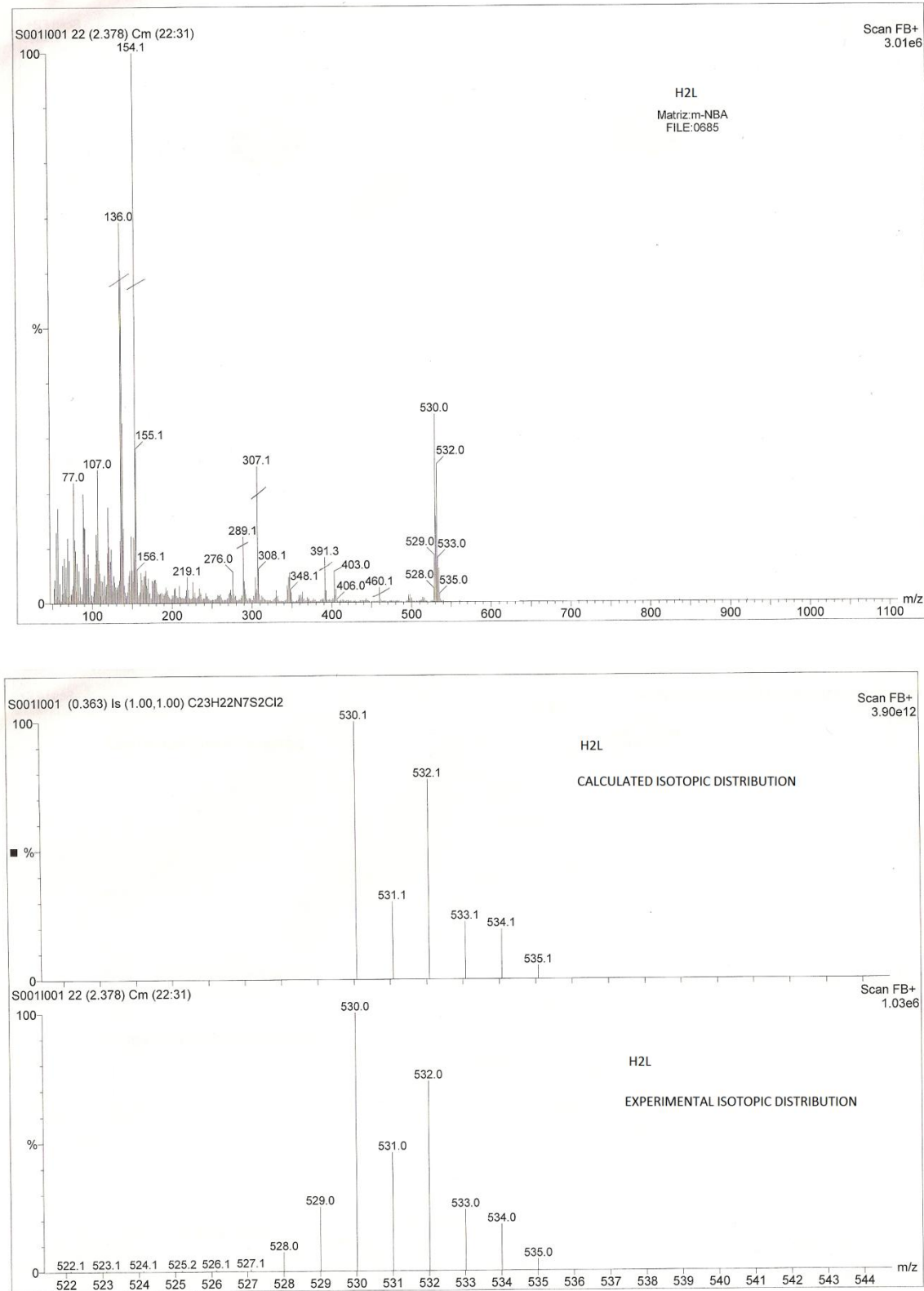


Fig. S1. MS spectrum for H₂L

Figure S2.

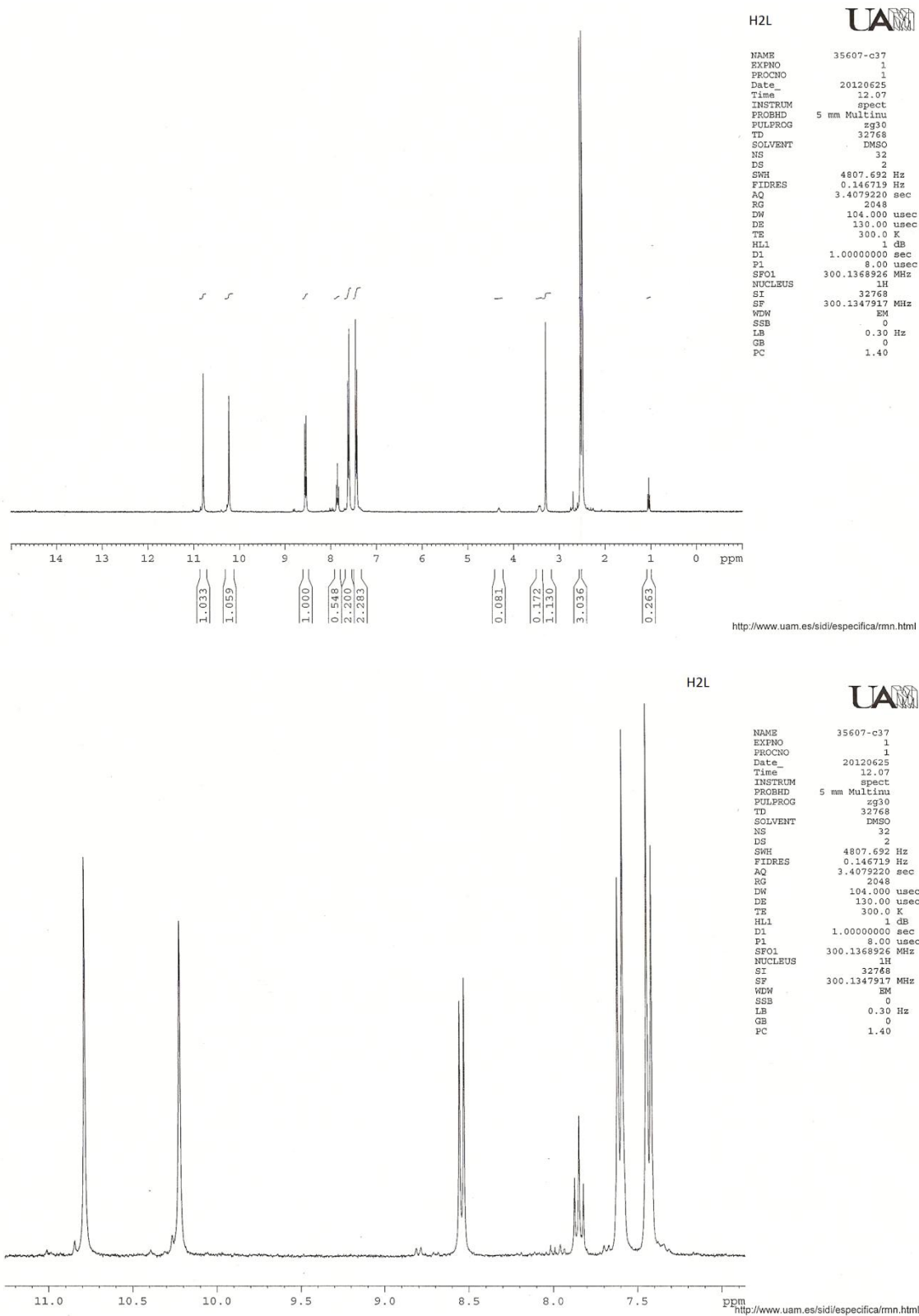


Fig. S2. ^1H NMR spectrum for H₂L

Figure S3.

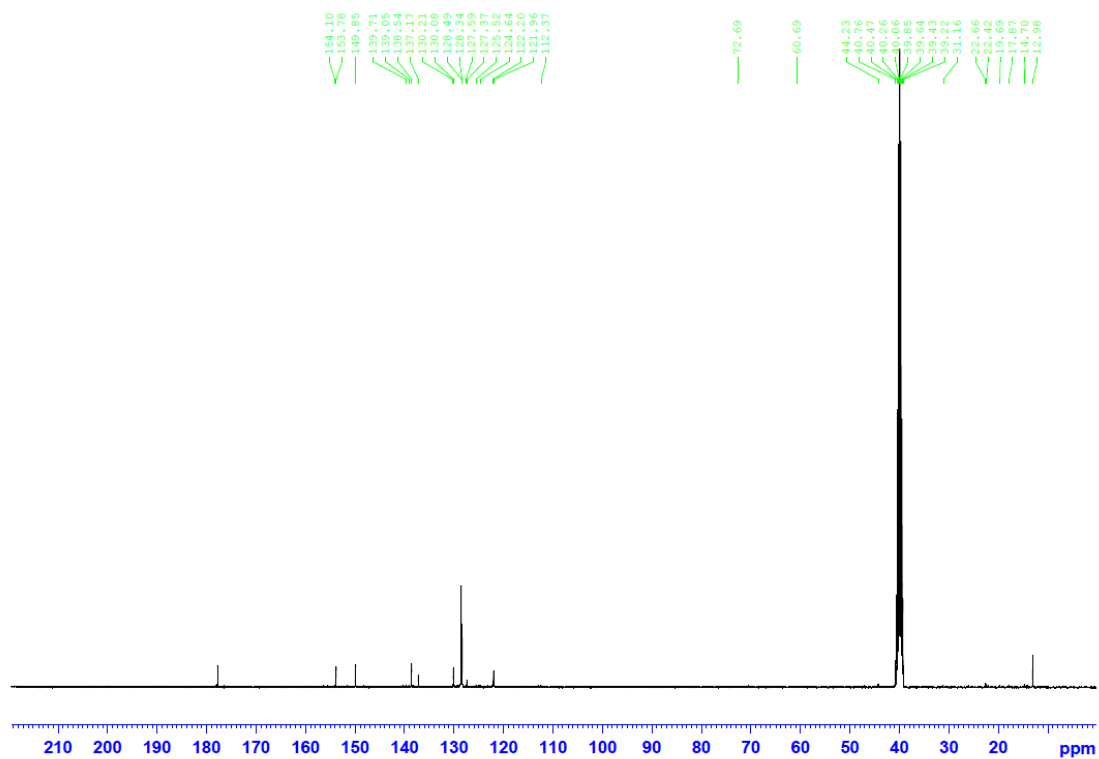


Fig. S3. ^{13}C NMR spectrum for H_2L

Figure S4.

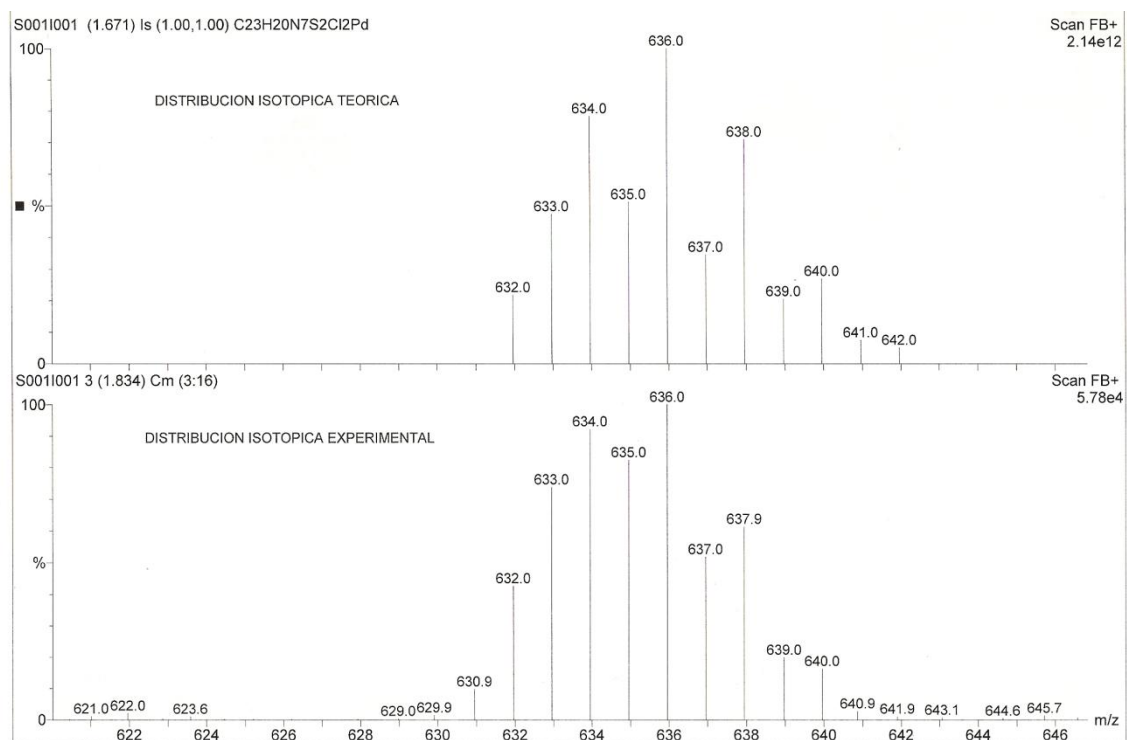
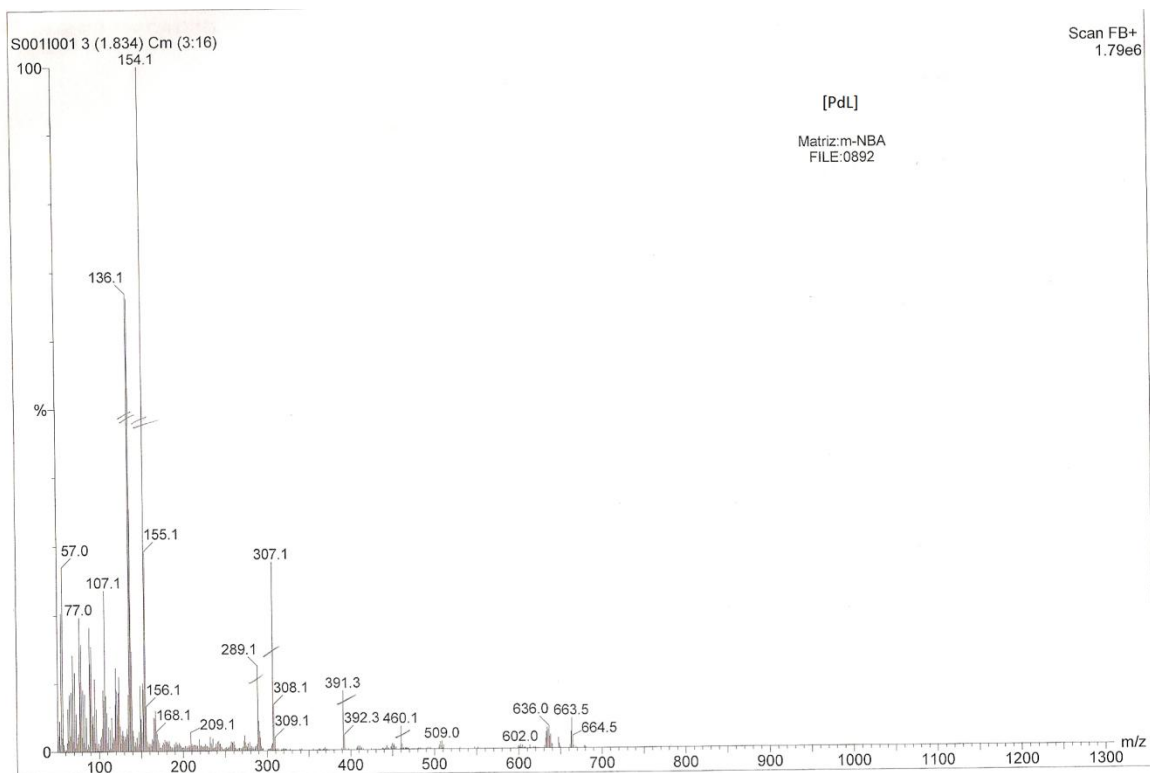


Fig. S4. MS spectrum for [PdL]

Figure S5.

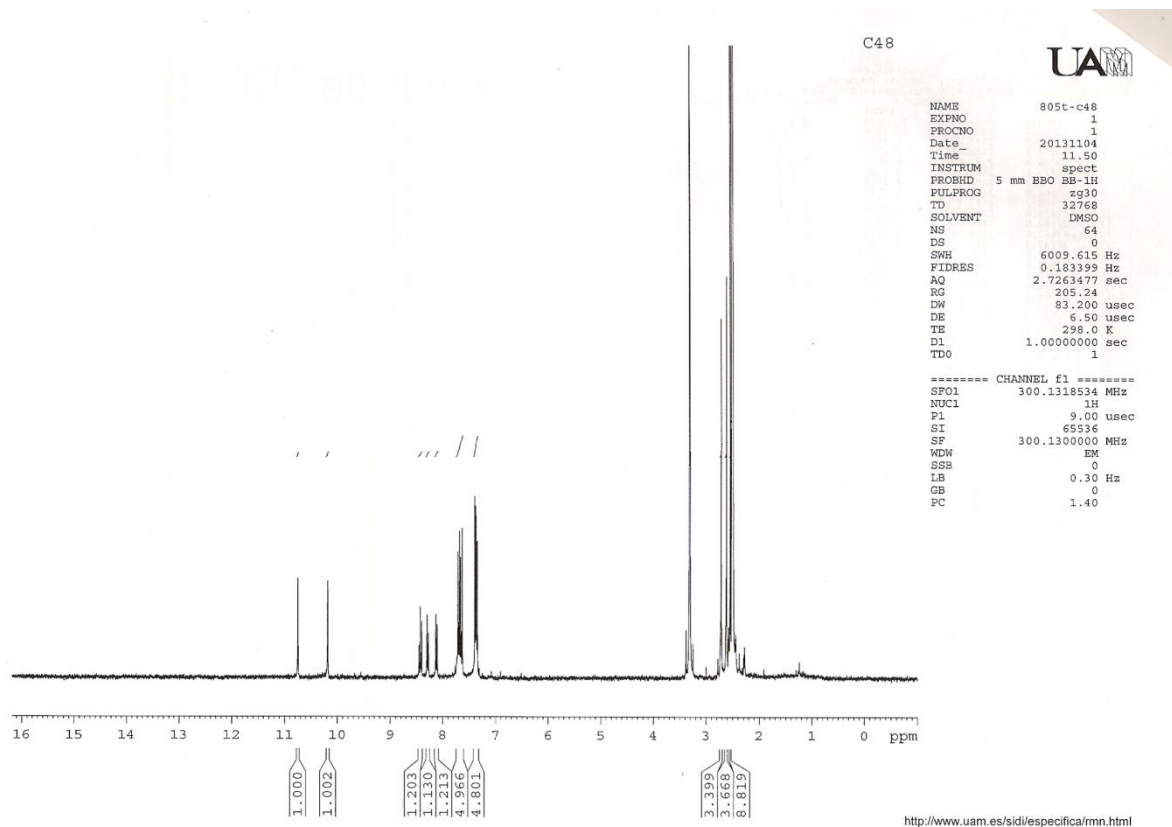


Fig. S5. ^1H NMR spectrum for [PdL]

Figure S6.

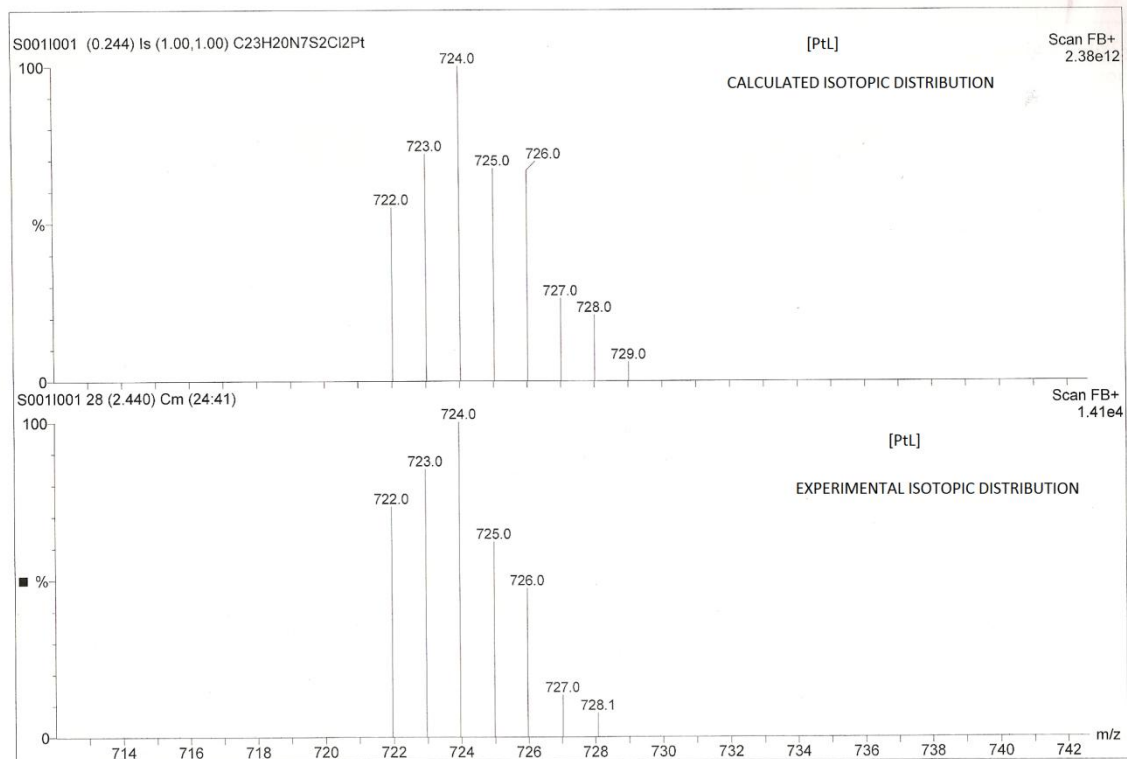
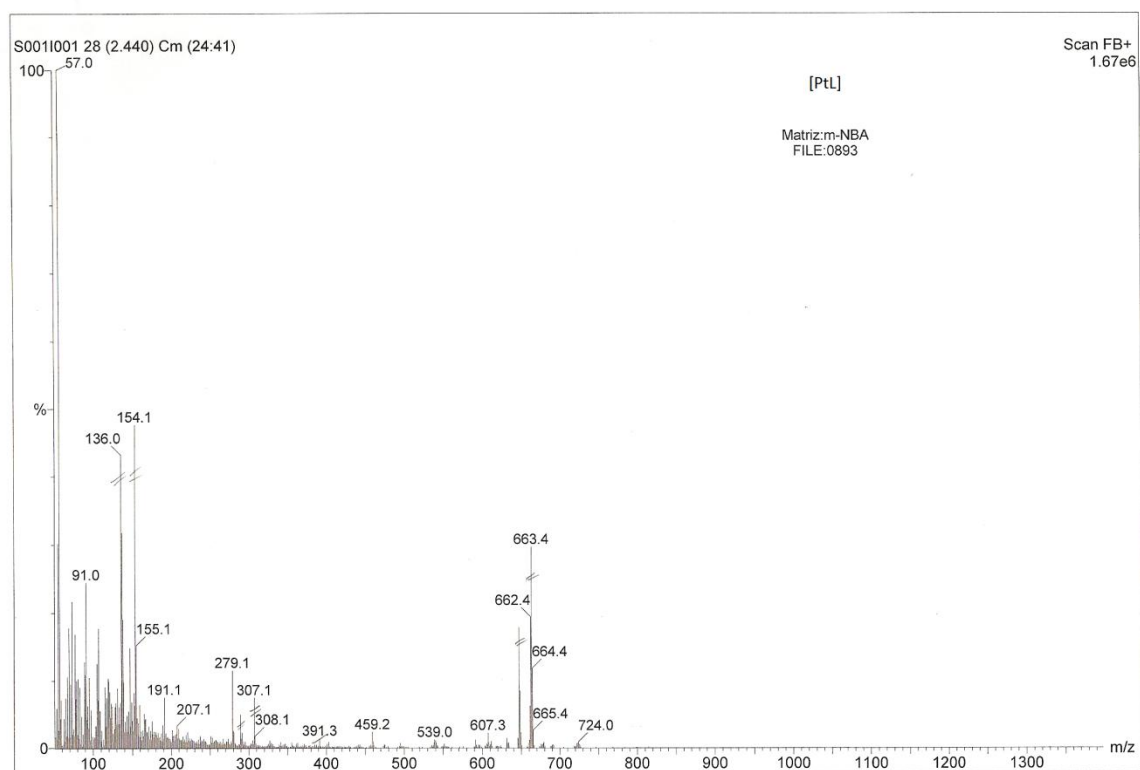


Fig. S6. MS spectrum for [PtL]

Figure S7.

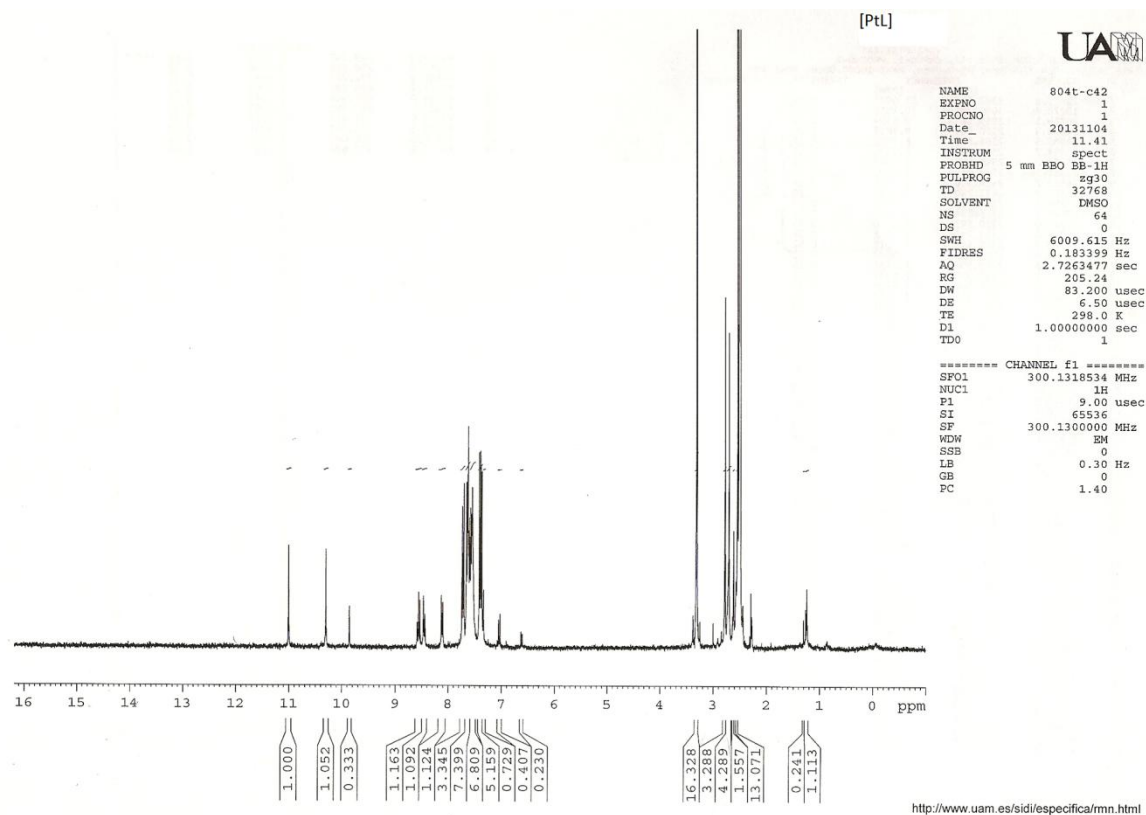


Fig. S7. ^1H NMR spectrum for [PtL]